Tampere University

Nanna Förster

FLUORESCENCE LIFETIME IMAGING FOR CHEMICAL SENSING

Faculty of Medicine and
Health Technology
Bachelor's thesis
November 2020

ABSTRACT

Nanna Förster: Fluorescence Lifetime Imaging for Chemical Sensing
Bachelor's thesis
Tampere University
Faculty of Medicine and Health Technology
Bachelor's Programme in Engineering and Natural Sciences, Bioengineering
November 2020

Fluorescence Lifetime Imaging Microscopy (FLIM) has become an important tool in biological research because it enables accurate and sensitive measurements of molecular level processes. FLIM is non-invasive, independent of a fluorophore's concentration, and sensitive to changes in molecular environments. There is a wide variety of FLIM techniques, including time-domain and frequency-domain methods which can be combined with widefield and scanning illumination options. Several methods are capable of optical sectioning but more advanced three-dimensional FLIM setups are still under development.

In this thesis, theory of fluorescence lifetime and principles of FLIM are reviewed based on literature search. The goal is to provide information about different FLIM methods and implementations, about how FLIM can be used in three-dimensional imaging, and about FLIM applications in cell biology and chemical sensing. First, fluorescence and fluorescence lifetime are introduced so that the reader can understand on what phenomena FLIM is based on. Time- and frequency-domain methods are described, current FLIM instrumentations are presented, and FLIM implementation possibilities to three-dimensional microscopy methods are considered. This is followed by an introduction to FLIM data analysis methods. Chemical sensing possibilities are examined by discussing FLIM applications for oxygen sensing, ion concentration measurements, pH monitoring and Förster resonance energy transfer measurements.

Literature reveals that there are many different approaches to determine fluorescence lifetimes. The decision about which method is the best depends on the application, desired lifetime accuracy, sample properties, and length of acquisition time. The review shows that also the used detector or camera affects the measurement outcome. By comparing different FLIM methods and detector types, it seems that megahertz frame rate cameras combined with time-domain approaches are most suitable for three-dimensional FLIM. Frequency-domain methods might be faster but less accurate. With the help of different analysis algorithms, fluorescence lifetime values can be determined from FLIM data. Moreover, noise and background signals can be reduced. This thesis reveals that FLIM has already been used successfully in many biological applications and that it can provide information of molecular environments. Future development might result in even more accurate and versatile FLIM methods which can be applied to image three-dimensional cell cultures and monitor their culturing conditions.

Keywords: fluorescence, lifetime, FLIM, three-dimensional imaging, chemical sensing

The originality of this thesis has been checked using the Turnitin OriginalityCheck service.

TIIVISTELMÄ

Nanna Förster: Fluoresenssin elinaikamikroskopia kemiallisessa tunnistamisessa
Kandidaatintyö
Tampereen yliopisto
Lääketieteen ja terveysteknologian tiedekunta
Tekniikan ja luonnontieteiden kandidaattiohjelma, Biotekniikka
Marraskuu 2020

Fluoresenssin elinaikamikroskopia (engl. Fluorescence Lifetime Imaging Microscopy, FLIM) on osoittautunut tärkeäksi työkaluksi biologisessa tutkimuksessa, koska se mahdollistaa tarkkojen ja herkkien mittausten tekemisen molekyylitason tapahtumista. FLIM on ei-invasiivinen tutkimusmenetelmä, joka fluoresenssin intensiteettimittauksista poiketen on riippumaton fluoresoivan molekyylin konsentraatiosta näytteessä. Olemassa olevien FLIM-tekniikoiden kirjo on laaja: aika- ja taajuustasoon perustuvia menetelmiä on yhdistetty niin laajakenttämikroskooppien kuin skannausmikroskooppien kanssa. Eri menetelmien soveltuvuus kuitenkin vaihtelee käyttökohteesta riippuen.

Tässä kandidaatintyössä perehdytään fluoresenssin elinajan teoriaan ja FLIM-menetelmien periaatteisiin kirjallisuusselvityksen pohjalta. Työn tavoitteena on selvittää, millaisia eri vaihtoehtoja FLIM:n käyttöönotossa on ja miten FLIM:ä voidaan hyödyntää kolmiulotteisissa mikroskopiamenetelmissä. Tarkoitus on myös esitellä FLIM:n sovelluskohteita solubiologiassa ja kemiallisessa tunnistamisessa. Työn alussa tutustutaan fluoresenssiin ja sen elinajan perusperiaatteisiin, jotta lukija hahmottaa, millaiseen ilmiöön FLIM pohjautuu. Sen jälkeen käsitellään aika- ja taajuustasoon perustuvia menetelmiä ja olemassa olevia FLIM-laitteistoja sekä kartoitetaan kolmiulotteisen FLIM-kuvantamisen mahdollisuuksia. Työssä esitellään myös lyhyesti FLIM-mittausten analysointia ja datan käsittelyä. FLIM:n soveltuvuutta kemiallisessa tunnistamisessa selvitetään tarkastelemalla sen käyttöä happipitoisuusmittauksissa, ionipitoisuuksien selvittämisessä, pH-arvojen määrittämisessä ja proteiinien välisten vuorovaikutusten tutkimisessa.

Kirjallisuusselvitys osoittaa, että on olemassa monia tapoja mitata fluoresenssin elinaikaa. Se, mikä mittausmenetelmä on paras, riippuu FLIM:n sovelluskohteesta, tulosten halutusta tarkkuudesta, näytteen ominaisuuksista sekä ajasta, joka mittauksiin voidaan käyttää. Työ paljastaa myös, että erilaisilla detektoreilla ja kameroilla voidaan vaikuttaa FLIM:n lopputuloksiin. Vertailemalla eri mittausmenetelmiä voidaan havaita, että kolmiulotteiseen FLIM-kuvantamiseen soveltuvat erityisesti megahertsien kuvataajuuksiin yltävät kamerat yhdistettynä aikatasomittauksiin. Taajuustasoon perustuvat mittaukset vaikuttavat olevan nopeampia, mutta vähemmän tarkkoja. Analysointialgoritmeja hyödyntämällä FLIM-datasta voidaan määrittää arvot fluoresenssin elinajoille sekä myös vähentää kohinasta ja taustasäteilystä johtuvia virheitä. Työ osoittaa, että FLIM-menetelmät tarjoavat luotettavia tapoja havaita molekyylitasolla tapahtuvia ympäristön muutoksia. Tulevaisuudessa FLIM:stä on mahdollista kehittää entistä tarkempi ja monipuolisempi mikroskopiamenetelmä, jota pystytään soveltamaan myös kolmiulotteisten solukasvatusten ja niiden olosuhteiden kuvantamiseen ja seurantaan.

Avainsanat: fluoresenssi, elinaikamikroskopia, FLIM, kolmiulotteinen kuvantaminen, kemiallinen tunnistaminen

Tämän julkaisun alkuperäisyys on tarkastettu Turnitin OriginalityCheck –ohjelmalla.

PREFACE

This work is a Bachelor's thesis done as a final project in the Bachelor's programme in Engineering and Natural Sciences for Tampere University. I would like to thank my supervisors Mart Kroon and Birhanu Belay for the valuable advices and support you gave me during this process.

In addition, I would like to thank my Bachelor's Thesis Seminar for guidance throughout the whole project. Thank you also to my friends who encouraged and supported me during this time. This autumn would have been much harder without you.

Tampere, 27th November 2020

Nanna Förster

CONTENTS

1. INTRODUCTION 1
2. FLUORESCENCE LIFETIME IMAGING BASICS 3
3. METHODS FOR FLUORESCENCE LIFETIME IMAGING 7
    3.1 Time-domain methods 7
        3.1.1 Time correlated single photon counting 8
        3.1.2 Gated image intensifier 10
    3.2 Frequency-domain methods 12
    3.3 Examples of current technologies 17
        3.3.1 Widefield FLIM 18
        3.3.2 Confocal-FLIM 18
        3.3.3 Multiphoton Microscope-FLIM 20
        3.3.4 Detectors currently used with lifetime measurements 21
        3.3.5 Implementation of FLIM into Selective Plane Illumination Microscopy and Optical Projection Tomography 26
4. FLUORESCENCE LIFETIME ANALYSIS 32
    4.1 Curve fitting methods 33
        4.1.1 Least square fitting 33
        4.1.2 Maximum likelihood estimation 34
        4.1.3 Global analysis 35
        4.1.4 Bayesian analysis 36
    4.2 Phasor method 37
5. CHEMICAL SENSING APPLICATIONS 39
    5.1 Oxygen level measurements 39
    5.2 Other applications 41
6. CONCLUSIONS 45
REFERENCES 48

LIST OF ABBREVIATIONS AND SYMBOLS

2D	Two-dimensional
3D	Three-dimensional
AC	Alternating Coupling
ACG	Asante Calcium Green
ACR	Asante Calcium Red
ADC	Analog-to-Digital Converter
DC	Direct Coupling
FLIM	Fluorescence Lifetime Imaging Microscopy
FRET	Förster Resonance Energy Transfer
GaAsP	Gallium Arsenide Phosphide
IC	Internal Conversion
IRF	Instrument Response Function
ISC	Intersystem Crossing
MCP	Multichannel Plate
OGB1	Oregon Green Bapta-1
OGB2	Oregon Green Bapta-2
OGB5N	Oregon Green Bapta-5N
OPT	Optical Projection Tomography
PLIM	Phosphorescence Lifetime Imaging Microscopy
PMT	Photomultiplier Tube
SPIM	Selective Plane Illumination Microscopy
TAC	Time-to-Amplitude Converter
TCSPC	Time-Correlated Single Photon Counting
TDC	Time-to-Digital Converter
TG	Time Gating

χ^2	chi-square
$D(t)$	detector gain at time t
E	energy
$E(t)$	excitation intensity at time t
f	frequency
$F(t)$	fluorescence intensity at time t
I	intensity
k_{IC}	rate constant of internal conversion
k_{ISC}	rate constant of intersystem crossing
k_{nr}	non-radiative rate constant
k_r	radiative rate constant
M	relative modulation
M_E	excitation modulation factor
M_F	emission modulation factor
ϕ	phase angle
Q	quantum yield
S	singlet state
τ	lifetime
τ_0	natural lifetime
τ_M	modulation lifetime
τ_p	phase lifetime
t	time
T	triplet state
ω	angular frequency

1. INTRODUCTION

Different microscopy methods are important tools for biological and biochemical research. In cell biology, especially fluorescence microscopy methods have turned out to be beneficial because fluorescence provides image contrast in otherwise transparent samples. The aim is to select only the objects of interest with fluorescent markers and to visualize them in an otherwise dark background [1]. Besides other fluorescence microscopy techniques, Fluorescence Lifetime Imaging Microscopy (FLIM) has gained attention in life science [2].

In the beginning, the number of FLIM studies was moderate but along with the development of microscopy instrumentation and analysis methods FLIM has become more and more popular. Especially after FLIM was demonstrated to be capable of measuring Förster Resonance Energy Transfer (FRET) in 1999, the number of publications including FLIM grew fast. Moreover, the commercialization of FLIM systems has increased the use of FLIM methods. [3, p. 147] The graph presented in Figure 1 visualizes the change in the number of FLIM publications over the past few decades. The most recent development is not shown.

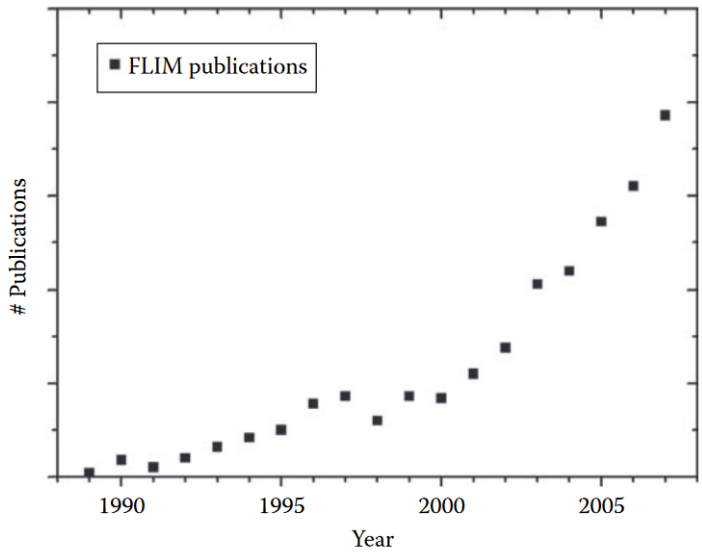

Figure 1. *Development of the number of FLIM publications during the last decades.* [3, p. 147]

Fluorescence microscopy methods are popular because they are non-invasive, non-destructive, sensitive, and provide structural information on molecular scale [4]. Lifetime imaging offers additionally insight into biochemical interactions and thus is capable of detecting differences in molecular environments [5]. Nowadays, there is a wide variety of different fluorescent molecules available which means that many different chemical sensing options are accessible with FLIM. The development of genetically coded fluorescent proteins has opened even more research possibilities. [1]

Knowing the basics behind fluorescence decay is necessary to understand and solve fluorescence lifetime imaging problems. Therefore, the aim of this thesis is to provide information about the principles of fluorescence lifetime and about how to acquire data of it. Based on literature search, my thesis gives an overview of how FLIM can be implemented to different microscope setups, how acquired lifetime data is analysed and what application options FLIM has. One specific interest will be FLIM implementations to three-dimensional (3D) imaging. The goal is to show how FLIM could be applied in 3D cell culture experiments.

This thesis contains four main chapters: chapters 2-5. Chapter 2 includes theory of fluorescence and fluorescence lifetime and explains why fluorescence lifetime measurements are better for imaging purposes than fluorescence intensity measurements. Chapter 3 has the main focus of this thesis. It provides information about different FLIM methods, reviews FLIM techniques and instruments that are currently used, and discusses FLIM implementation to 3D microscopy methods. In chapter 4, most common FLIM data analysis methods are introduced to see how actual fluorescence lifetime values can be gained from acquired FLIM data. Chapter 5 reviews different FLIM applications in the field of cell biology and chemical sensing, with oxygen sensing in the center of interest. In the end, chapter 6 summarizes the findings of this thesis.

2. FLUORESCENCE LIFETIME IMAGING BASICS

In general, molecules tend to be in the lowest energy states of their configurations. Such a normal low-energy state is called a molecule's ground state. For many molecules, the ground state is a singlet state *S* [3, p. 15] which is a molecular electronic state where electrons within an electron pair have opposite spins [2]. Another molecular electronic state is the triplet state *T* where an electron pair divides into two separate orbitals where the electrons have parallel spins. This configuration causes a magnetic moment that can align in a magnetic field in three possible ways; parallel, perpendicular, or antiparallel, which is also the origin of the triplet state term. [1]

Molecules can be excited from their ground state to higher energy levels called excited states. Normally, excited states do not last for long, but electrons return quickly to lower energy levels and eventually back to the ground state [5]. This de-excitation can be described as an energy loss which can be radiative (photon emission) or non-radiative [1]. The excitation and different de-excitation processes are presented in Figure 2 in an energy level diagram called Jablonski diagram.

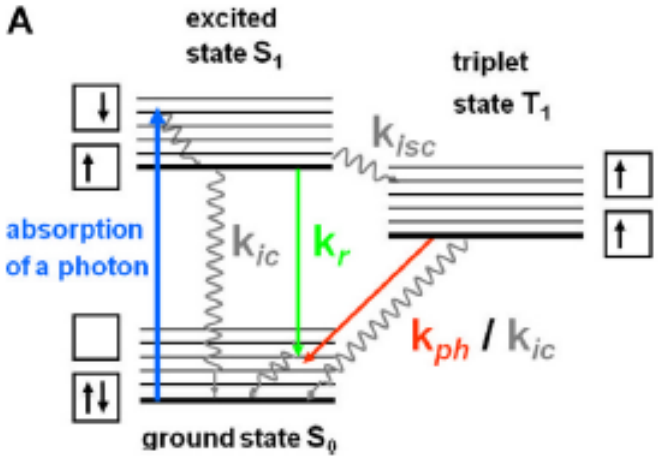

Figure 2. *Jablonski diagram. Blue arrow: photon absorption, green arrow: fluorescence decay, red arrow: phosphorescence decay, grey wave arrows: thermal relaxation, internal conversion and intersystem crossing events. Boxes on the sides illustrate orbits. The black arrows inside the boxes show electron spin states.* [2]

As shown in Figure 2, a molecule is excited from its ground state S_0 to a higher energy level S_1^x by absorption of a photon [2]. In the marking S_1^x, the 1 in the subscript refers to the first excited state, and the x in the superscript refers to the x^{th} vibrational level of that excited state. The molecule rapidly loses vibrational energy to the environment and ends

up in its lowest vibrational level of the first excited state S_1^0 [5]. *Fluorescence* is defined as the radiative de-excitation pathway in which the first excited state S_1^0 returns to ground state by emitting a photon (green arrow in Figure 2) [2]. Fluorescence is a spin-allowed process, meaning that the decay takes place from a singlet state to another. Thus, no spin flip is required. Therefore, the excited state is very short in fluorescence, ranging only from picoseconds to tens of nanoseconds. [3, p. 15]

Fluorescence is not the only pathway of de-excitation, but non-radiative decay mechanisms compete with the fluorescence pathway. One non-radiative decay example is *Internal conversion* (IC) which is a thermal relaxation process where the transition from an excited state to ground state takes place by converting the absorbed energy to heat [3, p. 10]. The excited molecule might also interact with nearby molecules and pass the energy to the molecular environment [4]. Such interactions with other molecules are, for instance, quenching or FRET [3, p. 12-14].

Furthermore, a molecule in an excited singlet state can go through *Intersystem crossing* (ISC). In ISC, the excited electron flips and changes the singlet state into a triplet state [3, p. 15]. Many molecules have triplet state vibrational energy levels that overlap with the singlet state energy level S_1. This overlap enables ISC even though the spin flip is a forbidden transition. [1] Like the singlet excited state, the triplet excited state can decay via non-radiative IC or radiative photon emission [3, p. 9]. The radiative decay from a triplet excited state to the singlet ground state is referred as *phosphorescence* (red arrow in Figure 2). Because a forbidden, and thus unlikely, spin flip is required in the phosphorescence pathway, the time before emission is longer than in fluorescence. Phosphorescence usually occurs microseconds to seconds after excitation. [5]

Each of the possible de-excitation pathways has its own rate constant that describes how likely a molecule will leave its excited state via that specific path. For fluorescence, the radiative rate constant k_r describes the probability per unit time that an excited molecule relaxes to ground state by emitting a photon [2]. The inverse of k_r defines the natural lifetime τ_0 of a fluorophore. The natural lifetime τ_0 describes the longest possible average time that the molecule can spend in the S_1 excited state when there is no other path for de-excitation and the molecule is isolated from interactions with other molecules [3, p. 8]. In practice, however, other de-excitation pathways and interactions with surrounding molecules do exist. These affecting factors are included in the non-radiative rate constant k_{nr} which is the sum of the rate constants for internal conversion k_{ic}, intersystem crossing k_{isc} and possible other de-excitation paths [2].

Fluorescence lifetime τ tells the average time that a molecule stays in its excited state before relaxation, and it is defined as the inverse of the sum of all available de-excitation pathways [2,3 p. 48]:

$$\tau = \frac{1}{k_r + k_{nr}} \quad (1)$$

where k_r is the radiative rate constant and k_{nr} the non-radiative rate constant.

Another measure of fluorescence emission is fluorescence quantum yield Q. It is a measure of fluorescence efficiency, telling the fraction of excited molecules that will relax trough the fluorescence pathway. In other words, it can be seen as the ratio of emitted fluorescence photons to the amount of overall absorbed photons. [2] The fluorescence quantum yield can be defined with the radiative and non-radiative rate constants as follows [3, p. 47]:

$$Q = \frac{k_r}{k_r + k_{nr}} \quad (2)$$

One can see that the fluorescence lifetime τ can now be expressed with the quantum yield Q and the natural lifetime τ_0 according to the following equation [2]:

$$\tau = Q\tau_0 \quad (3)$$

After defining fluorescence and fluorescence lifetime, decay characteristics of excited states in a molecule population can be examined. First, excitation will bring N fluorophores to their excited states. Within a time dt, a number of fluorophores dN return to ground state:

$$dN = (k_r + k_{nr})N(t)dt \quad (4)$$

where t is the time. Now when fluorescence intensity I is assumed to be proportional to the number of excited fluorophores, Equation 4 can be integrated and an equation describing the fluorescence intensity at time t is got [2]:

$$I(t) = I_0 e^{-t/\tau} \quad (5)$$

where I_0 is the fluorescence intensity at $t = 0$, and τ is the fluorescence lifetime from Equation 1. Equation 5 now shows that fluorescence intensity follows an exponential decay. Moreover, fluorescence lifetime determines the time in which the number of excited molecules, that is, the fluorescence intensity, decreases to 1/*e* (≈ *37%*) of the original value [5]. Here, *e* is Napier's constant (≈2.718).

Intensity-based fluorescence detecting is one of the simplest methods to measure signals from fluorophores. Fluorescence intensity depends on the number of emitted photons, in other words on the quantum yield of the fluorophore [1]. The more photons are

emitted, the higher the fluorescence intensity. This connection explains the dependency of fluorescence intensity on the concentration of the fluorophore [2]. Therefore, fluorescence intensity spectroscopy can be applied to measure unknown concentrations of fluorophores.

For imaging purposes, however, the dependency on the fluorophore concentration is not ideal. Especially in the case of biological samples where the fluorophore concentrations are rarely homogenous, intensity measurements can give non-uniform data. Additionally, intensity-based approaches are sensitive to background fluorescence, photobleaching of the fluorophore, and excitation source intensity [6]. Moreover, they cannot separate fluorophores with similar spectral characteristics or provide information of the dynamic molecular environment around a fluorophore [5].

FLIM has gained attention because it has several advantages over intensity-based methods. The lifetime of a fluorophore is independent on the fluorophore's concentration otherwise than in the case for intensity. FLIM can distinguish between fluorophores with similar spectral emission based on the fluorophores' lifetimes. Therefore, a wider selection of fluorophores is available for FLIM compared to intensity-based approaches, and thus, a wider range of parameters can be accessed with FLIM. [4] FLIM results are independent of light scattering which is advantageous when imaging biological samples. This aspect makes FLIM studies more reproducible and comparable with each other. [5] FLIM is able to provide information about the molecular environment of a fluorophore because fluorescence lifetime depends on the conformation of a fluorophore as well as its interactions with the environment. Conformational or environmental changes lead to changes in a fluorophore's fluorescence lifetime which can be detected and analysed. [4]

Even though FLIM has many advantages, it is more complex to implement compared to intensity-based imaging approaches. Therefore, it requires more knowledge about imaging principles, implementations, and data analysis methods. These aspects are reviewed in the next chapters of the thesis to get an overview how FLIM can be applied, especially in chemical sensing.

3. METHODS FOR FLUORESCENCE LIFETIME IMAGING

Acquisition of dynamic fluorescence lifetime information has two main approaches. One is based on time domain: the sample is excited with short excitation pulses and the fluorescence signal is measured directly as a function of time. The alternative method is based on frequency domain: excitation happens by a modulated excitation wave and the fluorescence response is determined with phase lag and demodulation of the emission wave in comparison to the excitation light. [2,5] This means that both time-domain and frequency-domain methods involve gathering information of the fluorescence time response and time-dependent decay, only in different domains. The relation can be seen in signal processing because time and frequency domains are finite Fourier transforms of each other [3, p. 24].

In the next two sections (sections 3.1 and 3.2), principles of time- and frequency-domain approaches are reviewed. Because both approaches can be implemented in a variety of ways, section 3.3 will concentrate on current techniques used in time- and frequency-domain FLIM. Different illumination techniques, available detector options, and implementation to several microscopy methods will be discussed.

3.1 Time-domain methods

In time-domain based methods, short-pulsed light is used for excitation of fluorophores. Fluorescence decay is recorded directly with photon counting detectors, and the photon counts or corresponding intensity values are saved in subsequent time channels. [5] This way, decay curves can be determined, and fluorescence lifetime values calculated.

One of the most used detectors for photon detection are photomultiplier tubes (PMT). PMT detectors consist of a photocathode and several dynodes inside a vacuum tube. When a photon hits the photocathode, electrons are ejected from the cathode surface. A potential difference between the cathode and the dynodes accelerates the electrons. The electrons hit the first dynode and that way generate more electrons. At each dynode, one electron can generate 5–20 secondary electrons depending on the voltage differences. The higher the voltage difference, the more electrons are generated and the more the original signal is amplified. All electrons are collected by an anode at the end of the

vacuum tube. The resulting anode current is proportional to the incoming light intensity. [7, p. 44]

PMTs can count photons individually or detect them as average emission signals. In single photon counting, photons are detected as electron bursts and measured as individual pulses. However, if two photons arrive at the same time, they are counted only as one. Simultaneous photon arrivals are not an issue in the analog PMT mode. There, individual pulses are averaged, and a mean photocurrent is measured. [7, p. 48] Thus, PMTs can be used in both time correlated single photon counting and in time gating approaches which are discussed next.

3.1.1 Time correlated single photon counting

Time correlated single photon counting (TCSPC) uses a high-frequency pulsed laser to scan a fluorescent sample [8]. Data is gathered by recording single photons of the fluorescence emission. The idea is to determine the time *t* from excitation until the arrival of each photon to the detector. This time information is used to construct a photon distribution over time. [9] The basic idea of TCSPC is presented is Figure 3.

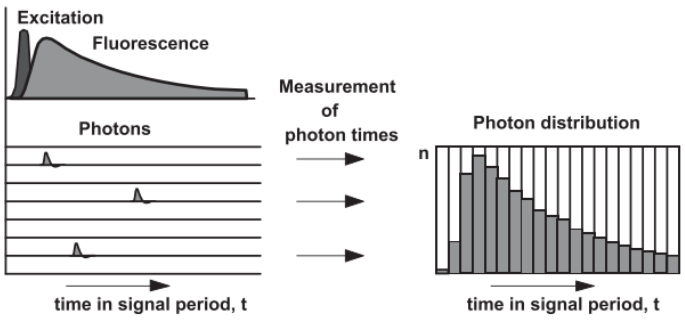

Figure 3. *Basic principle behind time-correlated single photon counting.* [10]

One-dimensional TCSPC records for each detected photon only the time difference between excitation and photon detection. Nowadays, however, multidimensional TCSPC approaches are available. These multidimensional TCSPC methods can determine other photon parameters as well. For example, the laser beam position at the moment of photon detection can be saved to spatial coordinates, *x* and *y* [4]. This way, a photon distribution over space and time can be acquired.

In a basic TCSPS approach, an optical pulse and an electrical pulse are generated at the same time. The electrical pulse goes to a time-to-amplitude converter (TAC) and functions as a start signal that initiates charging of a capacitor. Meanwhile, the optical pulse gets to the sample and excites it. Excitation is followed by fluorescence emission. The instrumentation detects only one emitted photon per excitation event. The detected

photon initiates a signal that stops the charging process in the TAC. The TAC gives out an analog signal which amplitude is proportional to the capacitor's charge and thus is proportional to the time past between the start and stop signals. [11] The TAC signal is digitalized by an analog-to-digital converter (ADC), after which the digital output is saved into a memory address [9]. An alternative for the TAC-ADC combination is to use a time-to-digital converter (TDC). In such cases, the time difference between start and stop signals is directly converted into a digital form [5]. In practice, TAC-ADC and TDC options do not have significant differences in working capabilities [3, pp. 148].

The principle described above functions in a forward manner where the reference pulse starts the timing and a detected photon stops the timing. An alternative approach is a so-called reverse start-stop geometry. There, the timing starts when a photon is detected and stops when a next reference pulse arrives [9]. This reverse method takes a system's dead time better into account. Dead time is the time needed to process the time information of one photon [8]. During that time, no other photons can be detected. Thus, the reverse start-stop mode is triggered only by usable photon events, not by reference pulses that do not result in any photon emission [3, pp. 148-149]. Therefore, it is beneficial especially if the laser repetition is high but photon count rates rather low [5].

In most TCSPC devices the time information of each photon is combined with spatial coordinates from the scanning area. A scanning interface constantly follows the position of the laser beam on the sample and thus provides spatial information [9]. With fast repetition excitation pulses, many pulses manage to arrive at each pixel before the laser scan continues to the next spot. Thus, several single photons are detected at each pixel. As a result of the scan, a three-dimensional array is got where each pixel contains its own fluorescence decay function. [7, p. 748] This principle is illustrated in Figure 4.

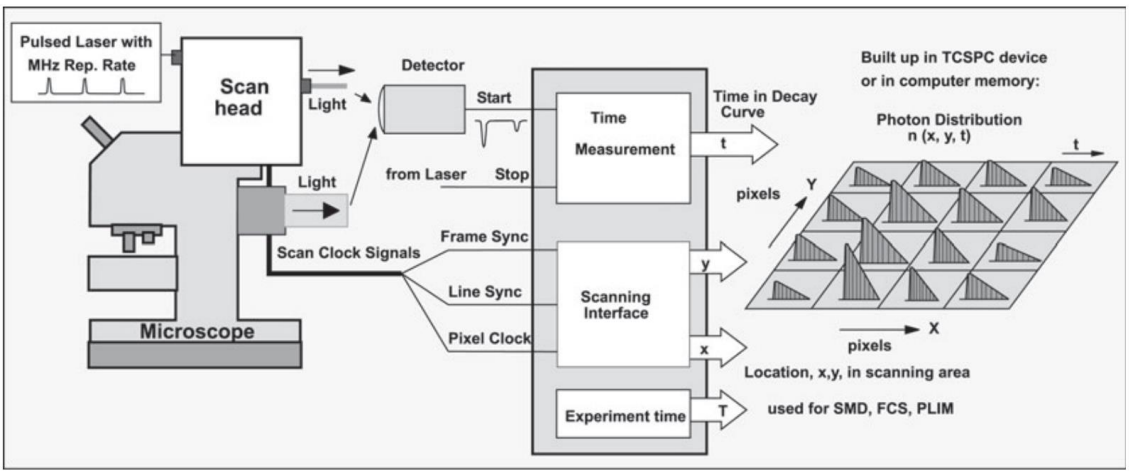

Figure 4. *TCSPC implemented with a laser scanning microscope.* [4]

Besides spatial coordinates, also the photon wavelength can be determined as an additional parameter. In such multi-wavelength FLIM systems, the fluorescence emission is spread over a detector channel array [10]. Based on the channel number where a photon is detected, the wavelength can be determined [4]. The acquired data can be described as shown in Figure 4, only that the decay functions in each pixel are additionally distributed over a wavelength spectrum.

TCSPC is one of the most used approaches used in FLIM. It is appropriate for high time-resolution measurements (up to picoseconds) with high efficiency requirements, and it has high lifetime accuracy [4,9]. It can be used for determining both single- and multiexponential decays [9]. Moreover, TCSPC has been described to have the best signal-to-noise ratios and a wide dynamic range [2].

Beside its advantages, TCSPC has also some limitations. For instance, TCSPC can be quite slow compared to other FLIM methods due to data acquisition pixel by pixel and photon by photon. In fact, the scanning rate of a FLIM system is usually the most limiting factor [4]. Moreover, acquisition times are affected by the required lifetime accuracy (how many photons need to be detected in each pixel), number of lifetime components, number of pixels, number of channels in the setup, and photon count rates of the fluorophore. That is why for accurate TCSPC measurements acquisition times are often quite long. [9] On the other hand, development of fast-scan-rate microscopes and multidimensional TCSPC have improved acquisition times significantly [10].

3.1.2 Gated image intensifier

Another time-domain based method that can be applied in FLIM is time gating (TG). The basic idea of TG is to collect intensity images at various time windows [7, p. 747]. Like TCSPC, TG also uses picosecond excitation pulses but emitted photons are not detected one by one. Instead, the fluorescence emission is directly detected in at least two time windows that are sequentially delayed from the excitation pulse. Photon numbers collected in the different time gated counters can then be used to determine the fluorescence lifetime. [3 p. 149,8]

One detector type commonly used in TG methods is image intensifiers. An image intensifier is a vacuum tube with a photocathode, a microchannel plate (MCP), and a detection system as shown in Figure 5a. When a photon hits the photocathode, it generates an electron which is guided into a channel of the MCP. There, the electron is multiplied into secondary electrons which continue their way along the voltage gradient and generate more electrons. At the other end of the channel, the electron burst hits a phosphor screen

where the electrons are converted back into photons. This way, low-intensity photon signals can be intensified before actual imaging. [4] As in PMTs, image intensifiers convert detected photons into electrons which then are multiplied. The difference lies in the output: a PMT's output is an electric current while an image intensifier's output is a photon signal.

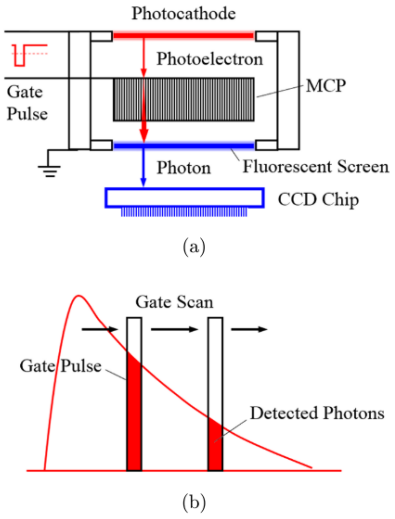

Figure 5. *a) Principle of an image intensifier. b) Time gating with two time windows.* [8]

Time resolution is got by gating the image intensifier with gating pulses [4]. The image intensifier is off when the photocathode is at a higher potential than the MCP inlet. In this case, the generated electrons do not reach the MCP and therefore, no signal is forwarded. If the photocathode has a lower potential than the MCP inlet, the electrons are driven to the MCP and intensification of the signal takes place. Usually, the MCP is held at a constant voltage and the photocathode is stimulated with negative gating pulses. [12] The width of the gating pulse determines the width of the time gate. Separate gates are delayed in different amounts with respect to the excitation pulse [8]. This way, intensity information of the fluorescence decay at sequential time points is obtained.

An example of TG with two time gates is given in Figure 5b. In such cases, the fluorescence lifetime can be calculated by [5]

$$\tau = \Delta t / (\frac{I_1}{I_2}) \tag{6}$$

where Δt is the time separation between the gates, and I_1 and I_2 are intensities measured at the two time gates. In Equation 6 the width of both gates is assumed to be same. Two time gates are enough to determine lifetimes of single-exponential decays [4]. For multiexponential decays, however, a two-window-system gives just an average fluorescence lifetime. Multiexponential lifetimes can be recorded by using more than two gates

which, on the other hand, requires more advanced data analysis methods and increases the acquisition time. [3, p. 149] Synchronized gating can be achieved, for instance, by applying separate gating pulses to the detector [8].

One advantage of TG is that it has faster acquisition times than TCSPC. Additionally, electronics of TG have shorter dead times than the ones in TCSPC so that TG can operate at high count rates. However, TG is less accurate than TCSPC and has lower time resolution. [2,5] Undersampling can be an issue, especially when using only two time gates [5]. Moreover, gating can result in situation where not all photons are detected which can lead to lower photon efficiency. Photon efficiency can be improved by designing the gate intervals to cover the decay curve as much as possible. [8] Accuracy can be improved by overlapping the time gates [7, p. 747].

3.2 Frequency-domain methods

Frequency-domain methods are based on the detection of phase shifts and demodulation occurring in the fluorescence signal. In comparison to time-domain approaches, in frequency domain the signal is an analogue waveform and not individually detected photon events [4]. Therefore, frequency-domain techniques are better to measure high intensities where single photons cannot be distinguished anymore [13]. Moreover, frequency-domain implementation might be easier than time-domain implementation because frequency-domain approaches do not require ultrashort pulsed lasers or complex timing electronics. On the other hand, frequency-domain methods might need more advanced analysis and can be susceptible to aliasing. [2]

Frequency-domain measurements make use of the fact that when a sample is excited with periodically modulated light, the fluorescence emission will have the same frequency but a different phase and amplitude compared to the excitation light [4]. The difference comes from the time that a fluorophore stays in the excited state [7, p. 159]. The modulated excitation signal can be expressed as [5]

$$E(t) = E(0)[1 + M_E \sin(\omega t)] \tag{7}$$

where $E(t)$ is the excitation intensity at time t, $E(0)$ is the excitation intensity at time 0, M_E is the excitation modulation factor, and ω is the angular frequency. The angular frequency is defined as

$$\omega = 2\pi f \tag{8}$$

where f is the excitation frequency. Often, excitation is sinusoidal and done at high frequencies in MHz range [5]. However, the light used for excitation has not to be sinusoidal. Actually, according to Liu et al., pulsed excitation is becoming the state of art in frequency-domain FLIM [8]. Anyhow, sinusoidal excitation is discussed here. Because a sinusoidal excitation will lead to a sinusoidal fluorescence response, the response can be described as follows [5]:

$$F(t) = F(0)[1 + M_F \sin(\omega t + \phi)] \tag{9}$$

where $F(t)$ is the fluorescence intensity at time *t*, $F(0)$ is the fluorescence intensity at time 0, M_F is the emission modulation factor, and ϕ is the phase lag between excitation and emission. The relative modulation M can be expressed as the ratio of M_F and M_E, which, on the other hand, are ratios of alternating coupling (AC) and direct coupling (DC) components of emission (Em) and excitation (Ex), respectively [5].

$$M = M_F/M_E = \frac{AC_{Em}}{DC_{Em}}/\frac{AC_{Ex}}{DC_{Ex}} \tag{10}$$

Phase lag and relative modulation values depend on the excitation frequency and on the time the fluorophore stays in its excited state. Therefore, ϕ and M can be used to determine fluorescence lifetimes. For single exponential decays, phase lifetime τ_p can be defined from [5,7 p. 99]

$$\tan(\phi) = \omega\,\tau_p \tag{11}$$

Similarly, modulation lifetime τ_M and the relative modulation M have a following relation [5,7 p. 99]:

$$M = \frac{1}{\sqrt{1+(\omega\tau_M)^2}} \tag{12}$$

Thus, by measuring the phase lag ϕ and relative modulation M between excitation light and emitted light, fluorescence lifetime can be determined. For single exponential decays, τ_p and τ_M do not differ from each other [5]. In the case of multiexponential decays, however, τ_p is usually smaller than τ_M, and the values will change depending on the modulation frequency [14]. Hence, comparison of τ_p and τ_M can be utilized to see whether a fluorescence decay is single- or multiexponential. In cases where the lifetimes differ, τ_p is preferred for determining fluorescence lifetimes [5].

Frequency-domain measurements are done over a wide frequency range. The relationship between the phase angle or modulation and the modulation frequency is called a sample's frequency response. [7, p. 160] Some example frequency responses are presented in Figure 6.

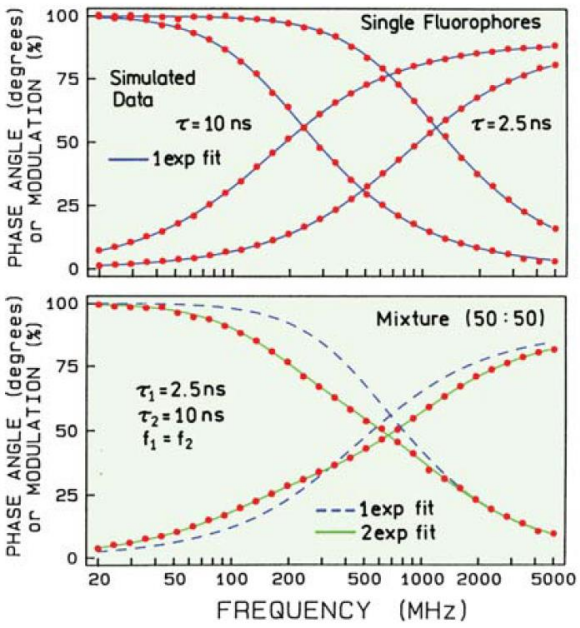

Figure 6. *Frequency responses for single exponential decay (top) and double exponential decay (bottom). When modulation frequency increases, phase angle increases but modulation decreases.* [7, p 160]

Figure 6 shows that the phase angle increases when modulation frequency is raised. On the other hand, when the modulation frequency is increased, the amplitude (modulation) of the emission becomes smaller. The range of frequencies needed to sample the frequency response of a fluorophore depends on the fluorescence lifetime. Measurements should be done at frequencies where the phase angles are frequency-dependent but the modulation amplitudes still measurable. For fluorescence lifetimes around 10 ns, a frequency range of 2–200 MHz is usually suitable. Longer lifetimes are determined in a frequency range of 10 kHz to 1 MHz, whereas shorter lifetimes in picosecond range require frequencies around 2 GHz. [7, p. 161]

The use of high excitation frequencies results in fluorescence signals with also high frequencies because the fluorescence signal $F(t)$ is a convolution of the excitation signal $E(t)$ and the fluorescence response $F_\delta(t)$ to a delta pulse excitation [15]:

$$F(t) = Q \int_0^t E(t')F_\delta(t - t')dt' \tag{13}$$

where Q is a constant that takes the material and instrumentation aspects into account [15].

Sampling high frequency signals is, however, more difficult than sampling low-frequency signals. To make frequency-domain FLIM instrumentation simpler and to avoid high-frequency noise, the fluorescence signal is converted into a low-frequency signal for detec-

tion. This is achieved by frequency mixing: the fluorescence signal is mixed at the detector with the excitation signal waveform. [3, p. 116] If the detector is modulated with exact the same frequency as the excitation has, the method is called homodyne [16]. If the detector is modulated with a frequency that differs from excitation a bit, the method is called heterodyne [4]. Both homodyne and heterodyne approaches preserve the phase shift and demodulation of the fluorescence in the mixed signal [3, p. 116]. The principles of homo- and heterodyne FLIM implementations are illustrated in Figure 7.

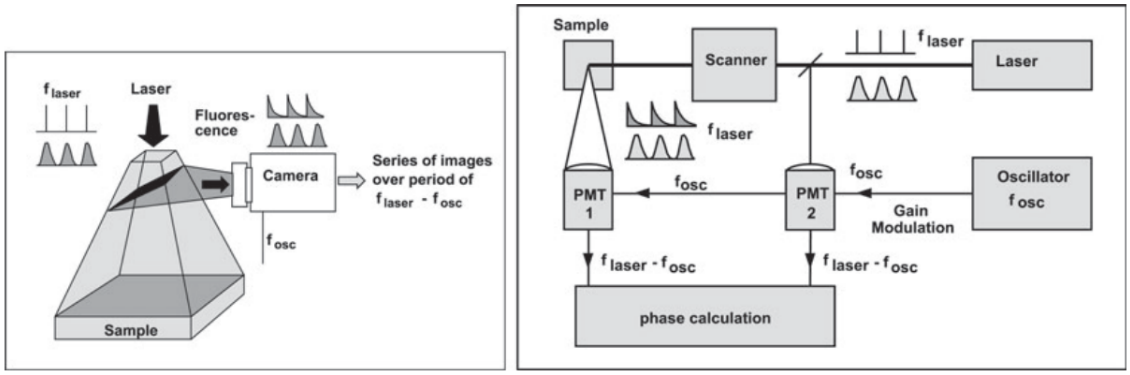

Figure 7. *Left: Homodyne frequency-domain approach with modulated camera detection. Right: Heterodyne frequency-domain approach with modulated point-detectors like photomultiplier tubes.* [4]

The homodyne method can be realised with gain-modulated image intensifiers [16]. The principle of the intensifier is the same as described for TG but the control signal applied to the intensifier's photocathode is different [8]. In TG, the photocathode was controlled by gate pulses. However, in homodyne frequency-domain approaches the gain of an image intensifier is modulated with a high-frequency repetitive voltage signal that has the same frequency as the excitation [3, p. 116]. Thus, the gain $D(t)$ of the detector can be expressed as follows [16]:

$$D(t) = D_0 + D\cos(\omega t - \phi_D) \tag{14}$$

where D_0 is the time average value (DC component) of the gain, D is the amplitude (AC component) of the corresponding signal, ω is the modulation frequency, and ϕ_D is the phase angle of the gain. The measured signal of a gain-modulated image intensifier is then the real-time product of the fluorescence signal $F(t)$ and the detector gain $D(t)$ [3, p. 122]. This output signal is averaged over a period of time *T* which results in a DC signal S_{avg} [16]:

$$S_{avg} = \bar{S}(\Delta\phi_{DE}) = \{F(t) \cdot D(t)\} = S_0(1 + \frac{M}{2}\cos(\Delta\phi_{DE} - \phi_F)) \tag{15}$$

where $\Delta\phi_{DE} = \phi_E - \phi_D$, and M and ϕ_F are the modulation and phase shift of the fluorescence, respectively. Eventually, S_{avg} images are collected at different phase offsets

$\Delta\phi_{DE}$. With the help of data analysis methods (described in section 4) the information of M and ϕ_F is got. The principle of this homodyne method implemented to frequency-domain FLIM is shown in Figure 8.

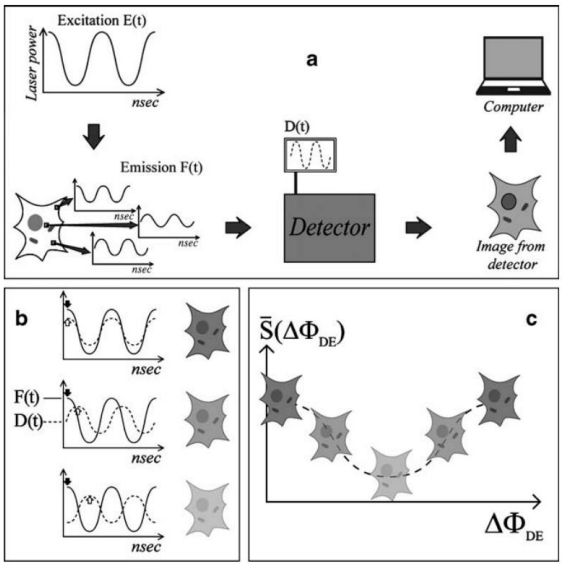

Figure 8. *Operation principle of the homodyne gain-modulation in frequency-domain FLIM. a) Emission from each point is detected by a gain-modulated image intensifier. The gain modulation has the same frequency as the excitation and a known phase delay. b) The fluorescence signal F(t) is multiplied with the detector gain D(t) at different phase delays of the gain. The averaged results correspond to the image intensities (represented by pictures on the right). c) The output signal S_{avg} is a function of $\Delta\phi_{DE}$.* [16]

Homodyne FLIM with a gain-modulated image intensifier is capable of fast image acquisition: several fluorescence lifetime images can be captured per second [17]. On the other hand, a disadvantage of image intensifiers is that they add noise to the data. The photoelectron multiplication step in an image intensifier amplifies the photon signals but also photon noise [17]. Still, frequency-domain FLIM systems with gain-modulated image intensifiers have been demonstrated to reach high modulation depths and have shown good sensitivity and gain [14].

While homodyne modulation is applied to widefield methods, heterodyne modulation is often combined with scanning techniques [16]. Because scanning techniques acquire data with point detectors like PMTs, the heterodyne approach is implemented by gain-modulating the PMTs with an oscillator frequency that differs slightly from the excitation frequency by δf. The result is a low-frequency signal at δf which carries the phase shift and demodulation information of the fluorescence emission [7, p. 164]. Excitation modulation and gain-modulation frequencies are changed so that δf stays the same, and the resulting phase shift and demodulation values are used to find out the fluorescence lifetime components [3, p. 116].

3.3 Examples of current technologies

Similarly as for FLIM data acquisition, there are two main principles for illumination: either scanning mode or widefield mode. In scanning mode, a focused beam illuminates the sample spot by spot, and the imaging data is collected to pixels sequentially. In widefield mode, the whole sample is illuminated simultaneously, and all pixels are measured at the same time. [5] In general, widefield methods are faster due to simultaneous illumination. On the other hand, the scanning mode is gentler to the sample because each spot gets overall less excitation radiation. Widefield methods do not require expensive scanning devices but need sufficient light sources that illuminate the whole field of view uniformly. [18] The decision of which mode should be chosen depends on the instrumentation and goals of each application. Figure 9 gives an overview on the setups of widefield and scanning FLIMs.

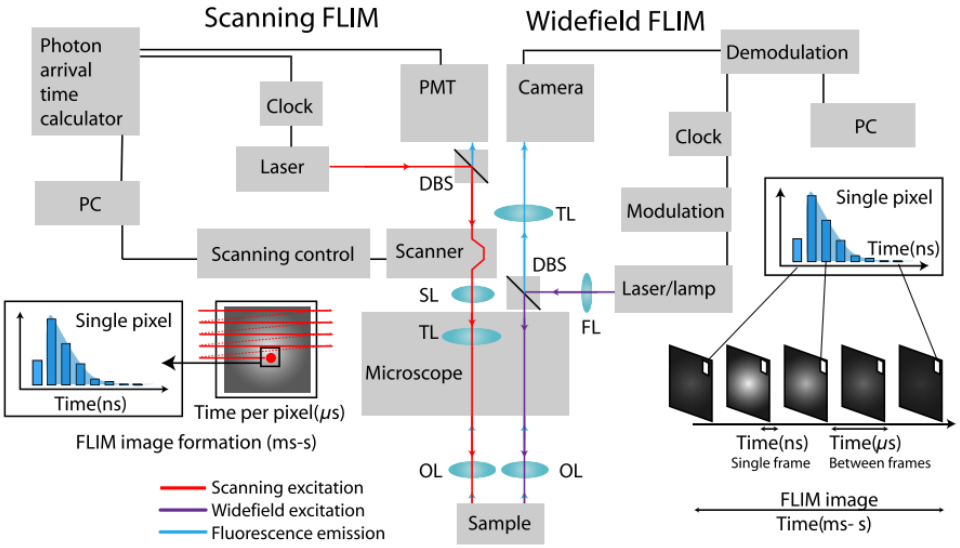

Figure 9. *Principle of FLIM implementation in scanning and widefield setups. Left: Scanning FLIM with TCSPC instrumentation. Right: Widefield FLIM with time gating instrumentation.* [5]

Independent of which FLIM method is used for imaging, the instrumentation needs to have some key features. First, a light source for illumination is required. Additionally, a sensitive detector must be incorporated to distinguish fluorescence photons from background noise. The electronics for photon arrival time estimation are also of great importance. [5] There are numerous strategies how to implement FLIM with different microscopes, and better and more sensitive solutions are developed constantly. In this thesis it is not possible to go through the wide variety of all different FLIM implementations completely. Instead, a few common implementations are discussed and possibilities of three-dimensional (3D) FLIM are reflected.

3.3.1 Widefield FLIM

Widefield FLIM is usually performed with time gating in time domain [8,19–21] or with gain-modulated image intensifiers in frequency domain [4,14,17]. As already mentioned, widefield FLIM approaches have the advantage of having faster acquisition times than scanning FLIM methods. The possibility of rapid imaging can be crucial in biomedical applications such as real-time cell imaging [2]. For instance, Agronskaia et al. [22] used a widefield FLIM setup with a time-gated image intensifier to acquire fast fluorescence lifetime data of calcium fluctuations in live myocytes. Their method achieved detection rates of 100 Hz, showing that time-gated widefield FLIM can result in high frame rates.

On the other hand, widefield methods do not reject out-of-focus light and lack therefore of optical sectioning capabilities [2]. Samples are also subjected to higher exposures which can cause photodamage or photobleaching. According to Wu et al. [23], photobleaching might be less problematic in frequency-domain widefield FLIM than in time-gated widefield FLIM because the frequency-domain widefield setups could acquire data even faster than the time-gated ones. Wu et al. presented a frequency-domain based setup containing a modulated camera for widefield fluorescence lifetime detection. Their setup was utilized to measure oxygen gradients in microfluidic channels [23].

Even though basic widefield methods lack of optical sectioning, research has been done to develop widefield techniques with 3D imaging capabilities. Optical sectioning characteristics can be achieved by discriminating out-of-focus light with additional techniques, such as structured illumination or single plane illumination [24]. As an example, Cole et al. developed a widefield setup for time-gated FLIM with an optical sectioning capability [25]. They applied a structured illumination technique with which they were able to image for instance fluorescent microspheres in 3D. The sectioned FLIM maps showed clear separation of individual spheres at different depth planes which was not achieved in conventional widefield FLIM maps [25]. Recently also TCSPC has been combined with widefield FLIM, combining the advantageous single photon sensitivity and accuracy of TCSPC with the fast and convenient widefield data acquisition [26].

3.3.2 Confocal-FLIM

Confocal microscopy is a scanning-based method where a pinhole is used to prevent out-of-focus light to get to the detector. Focused excitation light is used to scan the sample pixel-by-pixel. Only emitted light from the excited focus point gets through the pinhole and is recorded while light coming from other areas of the sample is blocked. By shifting

the sample position in an axial direction between individual scans, images can be acquired at many different planes and 3D information is obtained.

TCSPC is one of the most used FLIM techniques combined with confocal microscopes [5]. A standard confocal setup with TCSPC includes often a picosecond pulsed laser, a microscope scanning control (usually ready available in newer confocal microscopes), a suitable pixel clock and a PMT detection system [9]. Single photon detection suits well to pixel-by-pixel acquisition, and furthermore, TCSPC is compatible with the scanning rates of confocal microscopes [4]. Implementation of TCSPC in scanning FLIM has been reviewed for instance by Becker [4] and by Suhling et al. [2].

Here an example of a TCSPC-based confocal-FLIM given by Schoutteten et al. [27] is reviewed. As a light source, the group used a titanium-doped sapphire laser delivering picosecond pulses. The fluorescence emission was collected with an optical fiber and detected by a PMT. Time counting was done with a TAC in the reverse start-stop geometry, and the TAC output was digitalised with an ADC. Schoutetten et al. demonstrated fluorescence lifetime determination with temporal resolution of 37 ps. [27]

As in the case of widefield microscopes, confocal microscopes can also apply frequency-domain FLIM besides time-domain FLIM. Where a widefield frequency-domain FLIM included a gain-modulated camera system, a scanning frequency-domain FLIM applies gain-modulated point-detectors [4]. For instance, Booth & Wilson [28] used photomultipliers as detectors in their frequency-domain confocal FLIM setup. Excitation was done with a laser diode, and phase-sensitive detection was achieved by providing modulation with radio-frequency electronics [28].

Confocal-FLIM is not limited on TCSPC or modulated PMT methods. Time-gating has also been shown to be applicable in laser scanning microscopy: output signals from fluorescence emission detectors are guided into a number of gated counters that are sequentially open after each excitation pulse [29]. For instance in the study of Fereidouni et al. [30], a time-gated confocal setup with a gallium arsenide phosphide (GaAsP) photocathode PMT and a four-channel gating module was used to image FRET in fibroblast-like cells.

Even though confocal microscopy is usually based on scanning illumination, confocal approaches can be applied with widefield illumination methods, too. For instance, a spinning disk confocal head has been combined with a widefield FLIM setup to tackle the issue of long acquisition times due to the point-scanning procedure of conventional confocal microscopy [16]. The spinning disk setup is shown in Figure 10.

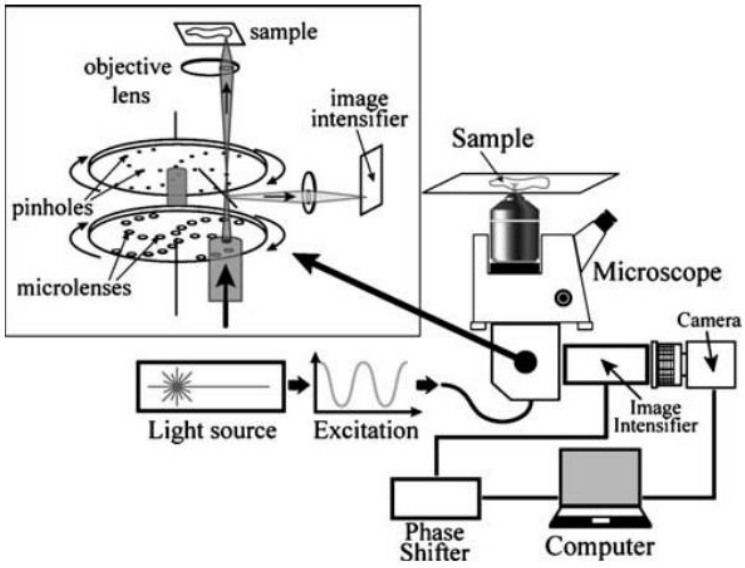

Figure 10. *Widefield FLIM setup with a spinning disc confocal head.* [16]

This setup includes a spinning disk with many pinholes arranged in a spiral pattern. A second disc containing microlenses splits the widefield excitation beam into about thousand small beams. The small beams are focused through the pinhole disc on the sample. Fluorescence emission from the sample travels through the same pinhole set which lets in-focus emission reflect on a dichroic mirror and further hit an image intensifier. The discs with the microlenses and pinholes rotate constantly, resulting in raster scanning of the sample which has clearly shorter acquisition times than basic confocal scans. Additionally, this approach enables 3D imaging in an otherwise 2D widefield setup. [16]

3.3.3 Multiphoton Microscope-FLIM

Multiphoton microscopy is another scanning microscopy technique. As its name reveals, it is based on excitation with more than one photon. One example is two-photon excitation. There, the energy of one excitation photon is half of the energy needed for excitation. To be excited, a single fluorophore must absorb two photons simultaneously because then the sum of absorbed photon energies equals to the excitation energy needed. Multiphoton microscope methods require high excitation photon densities so that simultaneous absorption can take place. [3, p. 43] Excitation is limited to a small volume without a pinhole because photon densities are high enough only in the spot in focus [5]. Because required photon energies are smaller than in one-photon excitation of confocal microscopes, excitation wavelengths used in multiphoton microscopy are longer. This leads to better depth penetration, reduced photobleaching and smaller photodamage in living samples [3 p. 41,31]. These are all beneficial aspects when imaging cell or tissue samples.

As for confocal-FLIM, TCSPC is one of the most used FLIM approaches combined with multiphoton microscopy [2,5,32]. Most multiphoton microscopes contain already a pulsed light source. Therefore, TCSPC-FLIM implementation to multiphoton microscopes requires usually only addition of timing electronics needed to estimate photon arrival times [5]. An example of TCSPC used with two-photon microscopy was presented by Gratton et al. [13]. They used a titanium-sapphire laser with a repetition frequency of 80 MHz and a pulse width of 100 ps to excite their samples. Fluorescence emission was detected with a PMT in photon-counting mode.

In the same study, Gratton et al. also showed an example of frequency-domain FLIM implemented in a two-photon microscope. The microscopy setup was the same as for the TCSPC measurements, except for the detector. For frequency-domain imaging, Gratton et al. utilized a gain-modulated PMT. Their cuvette and cell imaging experiments showed that their TCSPC technique had better signal-to-noise ratios at low fluorescence intensities but that the frequency-domain method was preferable for high intensity samples. [13] Another frequency-domain setup with multiphoton excitation and PMT detection was experimentally validated by Zhang et al. [33]. In their study, Zhang's group applied an analytical signal-to-noise ratio method to provide improved sensitivity over a wide fluorescence lifetime range.

Because multiphoton microscopy is based on scanning illumination, it has similar disadvantages concerning acquisition times as confocal-FLIM. Another issue in multiphoton microscopy is that optical aberration might increase when imaging depth increases. To tackle this issue, Coelho et al. combined adaptive optics to a two-photon FLIM system [31]. They tested their setup with FRET-FLIM measurements both *in vitro* with fixed cell samples and *in vivo* with live imaging of a mouse kidney and demonstrated that their approach showed improved resolution and lifetime accuracy.

3.3.4 Detectors currently used with lifetime measurements

Accurate detection and recording of emitted fluorescence photons are crucial for FLIM methods. FLIM requires detectors with high photon sensitivity and sufficient time resolution to capture nanosecond range fluorescence lifetimes effectively. To achieve as good FLIM images as possible, it is important to understand the capabilities and limitations of different detectors and cameras. In this part of the thesis, detectors and cameras commonly used in FLIM setups are reviewed. A summary of advantages and disadvantages is presented in Table 1.

Basically, scanning FLIM techniques usually require point detectors whereas widefield illumination methods are combined with camera-based detection. PMTs, which were discussed already above, are one of the most used point detectors in FLIM setups. They are small, reliable, and mostly inexpensive [2]. On the other hand, they have a low quantum efficiency [32] and they can be damaged if the emission intensities are too high [2]. Additionally, their transit time can be around 150 ps which is longer than a typical excitation pulse [9].

Other point detectors used in scanning FLIM are microchannel plates (MCP) and single photon avalanche diodes (SPAD). MCPs are similar to PMTs, only that they consist of plates with numerous small holes instead of a dynode chain. Photon detection generates electrons which drop inside the microchannels due to a voltage difference over the MCP, and the electrons are amplified as they travel through the channels. [7, p. 47] Because the electrons have only short paths to travel, MCPs have a clearly faster time response than conventional PMTs: MCPs can achieve time resolutions down to around 30 ps [9]. However, MCPs have usually lower amplification compared to PMTs [7, p. 47]. They are more expensive and also damageable by high intensity intensities [2].

SPADs are solid-state single-photon detectors that consist of a photodiode which p-n junction is reverse biased above its breakdown voltage. A single detected photon can generate an electron-hole pair that leads to an avalanche of second carriers. The voltage change across a SPAD during photon detection can be measured and converted into a digital signal. This output is compatible with standard electronics which is why SPADs are easy to combine to other circuit components. [34] SPADs can have transit times down to 40 ps. They are small, do not require high voltages to run, and are not easily damaged by high light exposure [26]. On the other hand, SPADs have only small active areas and they cause afterpulsing [2].

First SPAD detectors used in FLIM were based on time gating but the pixel architecture development has enabled SPADs to be applied in TCSPC FLIM as well [2]. For imaging purposes, SPADs are usually integrated into arrays which makes their technology more flexible and applicable with both confocal and widefield approaches [26]. SPADs' single-photon sensitivity, good spatial resolution, and picosecond time resolution make SPAD arrays a good alternative detector choice for dynamic cellular FLIM experiments.

To tackle issues that are present in PMT, MCP and SPAD detectors, hybrid detectors have been developed recently. Hybrid PMTs combine a PMT's photocathode with a silicon avalanche diode. Photoelectrons generated by the photocathode are accelerated over a high voltage difference to the diode. There they generate electron-hole pairs that

function as carriers and are amplified by the linear gain of the avalanche diode. One clear advantage of hybrid detectors is that amplification is done within one single step. This leads to output pulses with less amplitude fluctuation. [32] Furthermore, hybrid PMTs have low transit times of around 800 ps [8] and high counting efficiency [2]. Photons are not lost in absorption into the substrate which can be the case in conventional SPADs. Similarly, reflection of photoelectrons that can take place at dynodes of conventional PMTs is not an issue in hybrid versions. On the other hand, hybrid PMTs require high and stable voltages which can be hard to handle. [32] Anyhow, hybrid detectors have been stated to be the best point detectors currently available [2].

For widefield FLIM, camera-based detection is more suitable than the use of point detectors. One commonly used FLIM camera technique is based on charge-coupled devices (CCD). CCDs are pixel arrays where each pixel can accumulate charge in proportion to incoming light intensity. Pixel charges can be read out and used to construct 2D images. One CCD typically contains 10^6 pixels or even more. CCD cameras have a good sensitivity and a wide dynamic range. [7, p. 49] Then again, they can have low time resolutions which is why they are more practical for imaging probes with longer lifetimes [2].

In FLIM, CCD cameras are often coupled with image intensifiers to gate the camera's sensitivity in nanosecond range or to modulate it at radio frequencies [35]. CCDs combined with image intensifiers can be applied in widefield time-gated FLIM to acquire fluorescence intensity images at different time delays [21,25]. Modulated image intensifier -CCD combinations have been used for widefield frequency-domain FLIM measurements, as shown for example by Gadella et al. [14]. Their system had a time resolution of under 50 ps, a spatial resolution of around 400 nm, and fluorescence lifetime accuracies under 60 ps. Still, image intensifier -CCD setups require complex control, and time resolution can be limited by the performance of the image intensifier [18]. Therefore, also directly modulated CCD cameras have been studied to remove the image intensifier noise [35].

Table 1. Comparison of different detectors and cameras used in FLIM setups

DETECTOR / CAMERA	ADVANTAGES	DISADVANTAGES	REFERENCES
PMT	- single photon detection - small - reliable - inexpensive - much experience with implementation to FLIM	- low quantum efficiency around 10 % - damageable by high intensities - transit times can be long, around 150 ps → not optimal for subnanosecond lifetimes	[2,7 pp. 44-48,9,32]
MCP	- single photon detection - best time response: down to 30 ps - transit times only around 25-30 ps	- amplification lower than in PMTs - limited count rates - quantum efficiency around 10 % - expensive - damageable by high intensities	[2,7 p. 117,9,29]
SPAD	- single photon sensitivity - do not require high voltages to run - not damaged by high light intensities - high quantum efficiency around 70 % - transit times down to 40 ps	- small active area - afterpulsing - time-response can be intensity-dependent → not optimal for FLIM measurements with large intensity differences	[2,26,29,34]
HYBRID PMT	- outputs have small amplitude fluctuation - high count rates - photons are not lost in substrate material	- require high and stable voltage supplies - might be hard to handle	[2,32]
CCD	- sensitive - wide dynamic range - good quantum efficiency around 50-60 %	- expensive - low time resolution - performance can be limited by image intensifiers	[7 p. 49,18,35]
CMOS	- low power consumption - more cost efficient - up to MHz frame rates - wide dynamic range	- system response can be non-uniform	[18,23,26]
CMOS SPAD	- parallel single photon detection in pixels possible - noiseless readouts - high frame rates	- lower sensitivity especially in the red wavelength region - low active area - system integration can be more complex than with CCDs	[19,20,36]

In the past years, complementary metal-oxide-semiconductor (CMOS) image sensors have become an alternative for CCD cameras in FLIM applications [18]. CMOS consists of both n-type and p-type semiconductor field-effect transistors. Each transistor has a source and drain terminal as well as a gate which is isolated from the transistor body. A high enough voltage between the gate and body allows electrons to flow between the source and drain terminals. CMOS cameras seems to be easy to couple with FLIM set-ups and have been stated to be suitable for frequency-domain widefield FLIM [18,23]. Nowadays they reach MHz frame rates and can collect up to hundreds of photons per pixel [26].

An example of a CMOS camera used for frequency-domain widefield FLIM has been presented by Chen et al. [18]. The camera, QMFLIM2, contained 1008 x 1008 pixels with 5.6 µm pixel size, could be modulated up to 50 MHz, and had a quantum efficiency of 39 % and a maximum frame rate of 90 frames/s. The camera output consisted of a stack of modulated intensity images which were analysed with a phasor method. Chen et al. found out that their system had a non-uniform system response and a dependency of modulation signal on the intensity but with pixel level calibration they were able to carry out FRET-FLIM measurements successfully. [18]

CMOS technology can be combined with SPAD arrays, enabling parallelised data acquisition and thus implementation of single-photon counting to widefield FLIM [34]. For example, Li et al. [36] combined a 0.13 µm CMOS camera with a 32 x 32 SPAD array and implemented the combination to a widefield FLIM setup. Each pixel contained a TDC that enabled single photon recording. Li et al. tested their technique with fluorescent Rhodamine 6G beads and demonstrated video-rate FLIM performance with a frame rate over 50 frames per seconds [36].

Another example of a SPAD CMOS camera is SwissSPAD which has an array of 512 x 128 pixels. In this system, each pixel contains a SPAD and twelve transistors from which three form an in-pixel shutter circuit. A global high-speed signal is used to control these transistors to generate simultaneous shuttering for all pixels. In FLIM, the photons arriving during the global shutter period are counted, and the fluorescence lifetime can be determined from the measured signal. [37]

SwissSPAD2 was developed as an improved version of SwissSPAD. SwissSPAD2 consists of 512 x 512 photon-counting pixels that all have a SPAD with a gating mechanism and a 1-bit memory. Frame rates up to 97 700 binary frames per second can be achieved with this detector. Thus, SwissSPAD2 can improve time-gated widefield FLIM performance by increasing frame rates. [19] A SwissSPAD2 camera was used with widefield

FLIM by Ankri et al. [20]. They showed that their setup could detect fluorescence emission even through a tissue-like scattering and autofluorescent phantom layer. The method showed picosecond time resolution, high time-gating rates, and an acquisition time of 2.6 ms per gate. A phasor analysis method was used to successfully determine fluorescence lifetimes of the samples. [20]

It can be realised that there is not a perfect detector or camera for FLIM. Trade-offs need to be done depending on what are the most important requirements for each experiment. Time that is needed for data acquisition depends among others on photon efficiency of the technique, speed of used electronics, photon rate of the sample, and desired lifetime accuracy. Very accurate and fast setups are usually most expensive and might not be easily available. High time resolutions are needed when short lifetimes are imaged. For longer lifetimes (such as in phosphorescence) detectors with lower time resolution can be adequate. For example, CCD cameras can be suitable for µs range lifetimes but for ns lifetimes or shorter CMOS cameras that reach ps time resolutions might be preferable.

3.3.5 Implementation of FLIM into Selective Plane Illumination Microscopy and Optical Projection Tomography

As discussed previously in this chapter, confocal and multiphoton FLIM can offer optical sectioning capabilities and thus enable one kind of 3D imaging. These methods can provide high resolutions over a small volume but they have limitations when for instance millimetre-sized organs or tissue samples should be imaged. Confocal and multiphoton imaging have small field of views, long acquisition times and can lack in sensitivity. The more research interests are switching form 2D cell cultures to 3D cell studies and tissue engineering, the higher is the need for improved 3D imaging methods, also from the FLIM point of view. In this part of the thesis, two different 3D imaging methods are introduced and implementation of fluorescence lifetime imaging into these systems is examined.

The first 3D method discussed here is Selective Plane Illumination Microscopy (SPIM) where the idea is to apply a planar illumination to the sample. A sheet of light having a well-defined thickness illuminates the sample from the side so that only a thin sample layer is illuminated at a time. This way SPIM provides optical sectioning without creating out-of-focus light [38]. 3D data is collected by acquiring images at different Z-positions. In general, SPIM reaches high frame rates and has high signal-to-noise ratios. Compared to confocal and multiphoton microscopy techniques where scanning rates can be limiting, SPIM is more efficient when imaging large 3D volumes. Furthermore, SPIM can achieve deeper optical sectioning and causes less photobleaching or photodamage. [39]

In recent years, SPIM has been tested together with FLIM several times. An example of such an implementation has been given by Greger et al. [38]. They used a modulated laser diode for illumination, and fluorescence detection was achieved through a gain-modulated image intensifier coupled to a CCD camera. Their technique was based on a homodyne frequency-domain approach. The excitation source and the image intensifier were controlled by two frequency generators which modulated the laser and the intensifier with a same frequency but with a controllable phase shift. Figure 11 shows the setup used by Greger et al.

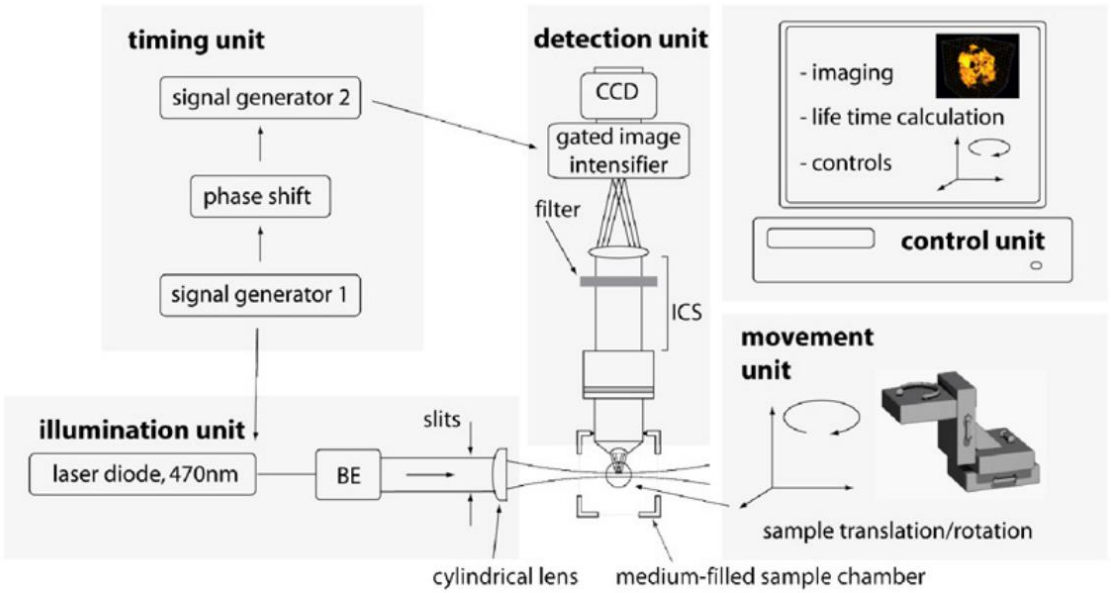

Figure 11. *The SPIM-FLIM setup presented by Greger et al.* [38]*. A beam splitter (BE) and a cylindrical lens form together the illuminating light sheet. Emission travels through an infinity corrected space (ICS), is filtered, and intensified before detection with a CCD camera. Frequency generators are responsible for the modulation of the laser and the intensifier.*

The system presented in Figure 11 was calibrated by measuring Rhodamine 6G lifetimes at different potassium iodide quencher concentrations. The system's capacity to measure fluorescence lifetimes in 3D was tested with different sized bead samples. It was shown that the setup distinguished fluorescence lifetimes along all three dimensions. Moreover, living Madine-Darby Canine Kidney cyst samples were successfully imaged. Greger et al. stated that SPIM-FLIM offers better signal-to-noise ratios and faster image acquisition of 3D fluorescence lifetime imaging than for example confocal or multiphoton microscopy. [38]

Instead of frequency-domain FLIM, also time-domain FLIM techniques have been implemented to SPIM. Funane et al. [40] tested a time-gated SPIM-FLIM approach whereas Hirvonen et al. [41] combined TCSPC with SPIM. The system of Funane et al. contained a frequency-doubled laser generation of a titanium-sapphire laser for excitation, and a

time gated image intensifier which output was collected by a CCD camera. The position in z-direction was controlled by a micromanipulator system with a smallest step size of 0.04 µm. Funane et al. tested their technique with microbead samples, and obtained successful fluorescence lifetime images from 3D cell cultures and cleared mouse brain samples. [40] Hirvonen et al. used a picosecond laser at 10 MHz repetition rate for excitation, and fluorescence emission was detected by a double MCP detector with a TCSPC module. The system was tested with fluorescent beads, after which it was applied to image human cancer cell spheroids and *C. elegans*. [41] An example of bead imaging results is shown in Figure 12.

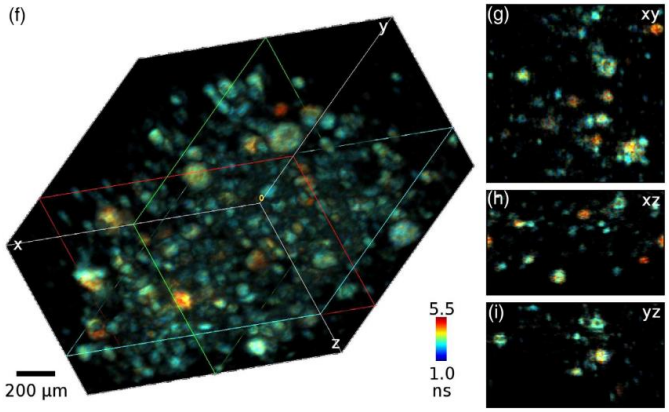

Figure 12. *Intensity-weighted 3D FLIM image with two types of fluorescent beads. Blue/green dots show beads with shorter lifetimes whereas yellow/red dots indicate beads with longer lifetimes. On the left, three cross-section images are shown. Modified from* [41].

Also Li et al. [42] implemented FLIM to a widefield light-sheet microscope. Instead of a static light sheet SPIM, however, they used a digital scanned laser light sheet microscope. Their setup contained a gated image intensifier which output was imaged with a 2048 x 2048 pixel CMOS camera. Time-gated fluorescence intensity images with different delay steps in respect to excitation were acquired at multiple depths. As a proof-of-concept, 3D FLIM images were taken from Rhodamine 6G beads and from live zebrafish embryos. [42] Similarly, Mitchell et al. [43] implemented FLIM in a digitally scanned light sheet microscope incorporating a CMOS camera. They applied frequency-domain measurements to achieve faster acquisition times compared to time-domain methods. In their study, Mitchell et al. demonstrated fast 3D fluorescence lifetime imaging of zebrafish larvae muscle [43].

The second 3D imaging method discussed here is Optical projection tomography (OPT). In OPT, projection images are taken from many angles around the sample, and a 3D result is calculated out of these images. The specimen is rotated precisely in determined angles and images are taken in every position. OPT can be used in two different modes.

In transmission mode, photons that come from an illumination source are detected on the other side of the specimen. In emission mode, fluorescent dyes are excited, and their emission is detected. [44] OPT-FLIM is run in in the emission mode. A 3D image can be constructed from the images taken around the specimen with a back-projection algorithm [44].

Before actual OPT-FLIM setups, a method for 3D fluorescence lifetime tomography imaging was presented [45]. Excitation was performed with a 100 MHz modulated laser diode, and fluorescence emission was collected with optical fibers. The fibers mounted the signals as 2D arrays on interfacing plates which were imaged by a gain-modulated image intensifier CCD camera. The system was successfully used to measure near-infrared fluorescence lifetimes of fluorophores that had been placed into breast tissue phantoms. [45]

One of the first FLIM implementations to OPT was introduced by McGinty et al. [46]. Their technique was based on widefield acquisition and time-gated fluorescence lifetime imaging. A fibre laser-pumped super-continuum-based light source was used for excitation. Fluorescence emission was intensified with a gated image intensifier and detected by a CCD camera. 10 time-gated images were taken at every projection angle. Images were acquired at 1° intervals. The setup can be seen in Figure 13. McGinty et al. tested their method with fluorescent beads and an antibody labelled mouse embryo. The results showed that fluorescence lifetime contrast is feasible for biological 3D imaging with OPT. [46]

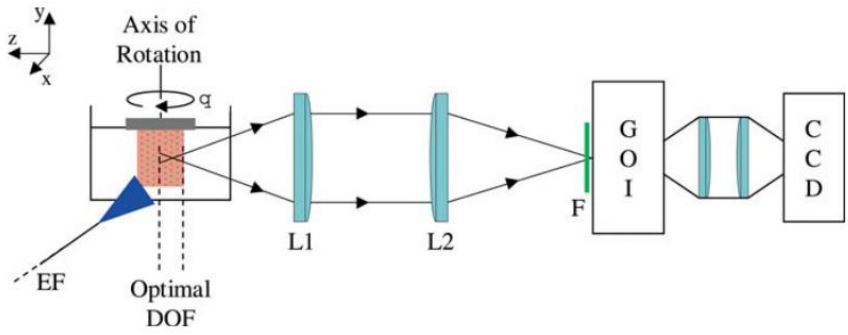

Figure 13. *FLIM implementation to OPT. EF: excitation fiber, DOF: depth of focus, L1 and L2: lenses 1 and 2, F: emission filter, GOI: gated optical intensifier, CCD: charge-coupled device.* [46]

A similar FLIM implementation to OPT was done by Andrews et al. to measure FRET activity in zebrafish embryos [47]. As in the setup of McGinty et al. [46], Andrews et al. used a fiber-laser-pumped super-continuum light source for excitation of the sample, and

a gated image intensifier connected with a CCD camera for detection of fluorescence emission. A series of 5 time-gated fluorescence intensity images was acquired at each projection angle. Andrews et al. reported that acquisition times were in the range of a few minutes to image a zebrafish embryo wholly. [47] Filtered back projection algorithm was used in both studies to construct the 3D intensity images for each time gate [46,47]. McGinty et al. determined fluorescence lifetimes for each reconstructed horizontal plane with an iterative fitting algorithm [46]. In the study of Andrews et al., an in-house software, *FLIMfit*, was used to determine fluorescence lifetimes in each voxel [47].

OPT and SPIM are both widefield techniques and require therefore a camera detection system for data acquisition. This chapter has shown that widefield FLIM data in general is often acquired with CCD cameras. Furthermore, research presented in this subchapter reveal that CCD cameras combined with image intensifiers have been successfully applied in both SPIM-FLIM and OPT-FLIM: the SPIM-FLIM techniques used either time gating [40] or frequency-domain approaches [38], and the OPT implementations utilized the time gating method [46,47]. Thus, it seems that a CCD camera is a suitable choice when implementing FLIM to SPIM or OPT. More detailed implementation explanations can be found in the articles introduced above.

Due to recent camera development, CMOS cameras might provide an interesting alternative for the CCD-based technologies. It seems that CMOS sensor solutions start to replace CCD cameras in microscopy setups, and this trend starts to be observable also in 3D FLIM implementations. Besides CCDs, it has been demonstrated that CMOS cameras are applicable to both time-gated SPIM-FLIM and frequency-domain SPIM-FLIM [42,43]. Above it was demonstrated that CCD cameras are suitable for both SPIM and OPT. So, if CMOS cameras are integrated with SPIM, it could be assumed that they can be applied to OPT as well.

As SPIM and OPT are widefield-based microscopy methods, it is logical that they have been tested first with time-gating and frequency-domain methods. However, the development of widefield TCSPC methods is interesting for camera based FLIM setups, including SPIM and OPT. TCSPC might be preferable for SPIM-FLIM and OPT-FLIM because of its good signal-to-noise ratio, picosecond time resolution and single photon sensitivity. Moreover, TCSPC has good performance also at low photon counts which might be common in 3D imaging with SPIM or OPT.

In general, widefield TCSPC is mostly based on MCPs or SPAD arrays [26]. Hirvonen et al. [41] demonstrated that TCSPC can be integrated to SPIM by using MCPs. In addition to MCP and SPAD detectors, also CMOS cameras in combination with photon counting

image intensifiers have been utilized for TCSPC [26]. Thus, if TCSPC is required in a SPIM-FLIM or OPT-FLIM experiment, CMOS could be the camera of choice. Moreover, camera based widefield TCSPC has been stated to be well suitable for acquiring phosphorescence lifetimes [26], which is interesting when considering for instance oxygen sensing based on phosphorescence quenching.

The problematic thing with TCSPC implementation to SPIM and OPT is the acquisition time and amount of data. Already 2D TCSPC setups might struggle with slow acquisition times and large data sets. When the imaging method changes from 2D to 3D, even more information is collected, and more time is required. Again comes the question, what parameter is most important for the experiment. If high quality and lifetime accuracy are emphasized, then TCSPC might be the best choice even for SPIM or OPT. On the other hand, if fast acquisition is required and samples have high photon counts, then time gated or frequency-domain FLIM should be considered.

4. FLUORESCENCE LIFETIME ANALYSIS

To fully understand a FLIM process from data acquisition to final fluorescence lifetime results, it is useful to understand basics of FLIM data analysis as well. As we have seen, time-domain data are pixel arrays where each pixel contains multiple time channels. The time channels include photon counts for consecutive times after excitation. To access fluorescence lifetime values from data like this, a designed decay model is convoluted with the instrument response function (IRF) [5]. The IRF describes how the used detection system responses to the applied excitation pulse. Iterative fitting algorithms optimise the decay model parameters until a proper fit to the photon distribution data is achieved [4]. The fitting procedure is repeated for all pixels.

FLIM images are constructed by giving each pixel a brightness corresponding to the total photon number in the pixel, and by giving it a color corresponding to the determined decay parameter [4]. An example of such time-domain analysis is shown in Figure 14.

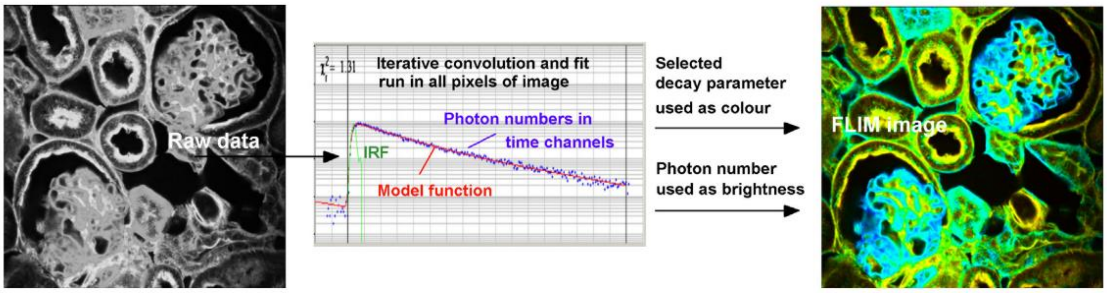

Figure 14. *A decay curve model is iteratively fitted to each pixel of the TCPSC data. Brightness of pixels in the resulting FLIM image corresponds to detected photon numbers, and the color corresponds to a selected decay parameter, mostly the fluorescence lifetime.* [10]

Not all FLIM data analysis methods are based on fitting a model to the experimental data. Fit-free methods have been developed to avoid the iterative steps needed in fitting algorithms [5]. An example of fit-free tools is the phasor method which is commonly used to analyse frequency-domain FLIM data. Frequency-domain data contains in each pixel a value for phase shift and for modulation degree [4]. The phasor method uses these values directly and displays them on a polar plot [16].

In the following sections, some common FLIM data analysis methods are shortly reviewed. Besides them, there are plenty of other analysis tools as well and new ones are constantly developed. More detailed comparison of different analysis methods has been given for instance by Datta et al. [5] and Liu et al. [8].

4.1 Curve fitting methods

The principle behind curve fitting is to find a decay function that fits well to detected photon histogram data. To run curve fitting analysis, some assumptions are required: the number of lifetime components, the temporal offset of the detected signal, and sources of background fluorescence need to be known. Based on the assumptions, a decay model is designed and convolved with the IRF of the system. The resulting decay is compared to the experimentally measured decay. A chi-squared (χ^2) goodness-of-fit test is often performed to see how well the model describes the experimental data. The goal is to achieve a fit that describes the experimental values as accurately as possible. [5]

Several approaches to perform curve fitting have been developed. They all describe how likely it is to detect a specific photon count in the time windows of the experimental decay but are based on different statistical approaches [5]. Four different curve fitting methods are discussed next.

4.1.1 Least square fitting

Least square fitting starts with choosing an assumption for a proper decay model. Most commonly, the fluorescence intensity decay described in Equation 5 is used. Because in time-domain the fluorescence intensity is directly related to the photon counts, the number of counts per unit time $N(\alpha, t)$ can be expressed as [3, p. 346]:

$$N(\alpha, t) = N_0 e^{-t/\tau} \tag{16}$$

where α is a vector of fitting parameters of the fitting function, N_0 is the photon count at time zero, and τ is the fluorescence lifetime. When $N(\alpha, t)$ is convoluted with the IRF $L(t)$, a calculated decay $N_c(t_k)$ can be determined [3, p. 347]:

$$N_c(t_k) = \int_0^{t_k} L(t_k - t) N_0 e^{-t/\tau} dt \tag{17}$$

where t_k is the kth time interval. The calculated decay has two fitting parameters: N_0 and τ. To find the parameter values best describing the actual decay, the calculated decay $N_c(t_k)$ is compared with the measured data $N(t_k)$. This is done with the χ^2 goodness-of-fit test which is described by [7, p. 130]:

$$\chi^2 = \sum_{k=1}^{n} \frac{1}{\sigma_k^2} [N(t_k) - N_c(t_k)]^2 \tag{18}$$

where n is the number of time channels or data points used in the measurements, and σ_k is the standard deviation of each data point. The value of χ^2 is dependent on the

number of datapoints. Therefore, the reduced χ^2 value χ_R^2 is used to estimate the quality of the fit [3, p. 348]. The reduced chi-square χ_R^2 is defined as

$$\chi_R^2 = \frac{\chi^2}{n-p} = \frac{\chi^2}{v} \tag{19}$$

where n is the number of data points, p is the number of fitting parameters, and v is the degree of freedom [7, p. 131]. Different numerical algorithms have been developed to minimize the squared difference between the measured fluorescence and the estimated fit. The closer χ_R^2 is to value 1, the better is the fit.

One advantage of least square analysis is that it is easy to implement. The method is especially used in TCSPC approaches where the data often fulfils the required assumptions. Moreover, TCSPC can reach good signal-to-noise ratios. This is convenient for least square analysis because its accuracy gets better when the signal-to-noise ratio of the data increases. [5] Least square analysis can be applied for frequency-domain FLIM data as well. However, independent of which domain the data has, least square analysis gets slow when images start to have more than 10^5 pixels [13].

4.1.2 Maximum likelihood estimation

The basic idea behind maximum likelihood estimation is to find model parameters that maximise the likelihood of a descriptive model to produce data that corresponds to the experimental measurements [8]. As in the case of least square analysis, also maximum likelihood estimation requires a proposed model for the fluorescence decay behaviour. The difference is that least square analysis consists of two fitting parameters whereas maximum likelihood estimation depends only on the fluorescence lifetime τ [48]. The lifetime that is most likely the correct one can be determined from [7, p. 124]:

$$1 + \left(e^{\frac{T}{t}} - 1\right)^{-1} - m\left(e^{m\frac{T}{t}} - 1\right)^{-1} = N_t^{-1} \sum_{i=1}^{m} iN_i \tag{20}$$

where m is the number of time windows in the decay profile, N_t is the photon count of the decay, N_i is the photon count in time window i, and T is the width of the time window. The maximum likelihood estimation does not use χ^2 as a goodness-to-fit parameter but instead has an own quality parameter $2I^*$ which can be defined as [48]:

$$2I^* = 2\sum_i^m N_i \ln\left(\frac{N_i}{g_i}\right) \tag{21}$$

where g_i is the model value in time window i described by the proposed model g.

Both least square analysis and maximum likelihood estimation are suitable for high photon counts [5]. Experimental evidence shows that these two methods seem to become

equivalent when photon counts are above 20 000, but that least square analysis results get inaccurate at photon counts below 20 000 [48]. Namely, least square analysis assumes that the noise is Gaussian-distributed which is not true for low photon counts [3, p. 347]. Maximum likelihood estimation uses a Poisson-distributed noise assumption which works also at low photon count rates. For this reason, maximum likelihood estimation is a better choice for low photon count data. [48]

4.1.3 Global analysis

Least square analysis and maximum likelihood estimation methods analyse FLIM data pixel by pixel which can get time-consuming for large data sets. Global analysis was developed as an alternative analysis approach for per pixel methods [30]. In global analysis, some model parameters are assumed to be the same in all data sets. In the case of FLIM data, the idea is to assume that there is no spatial variation in lifetime values, hence that the lifetimes are same in each pixel [49]. This means that all pixels are analysed simultaneously and single lifetime values are determined for all data points. Only the fractions of different fluorescent molecular species varies over the sample [3, p. 374].

Simultaneous analysis of pixels is accomplished by summing over N harmonic frequencies and M pixels in the image. The goal is to minimise the following χ^2 measure [49]:

$$\chi^2(a_{q,m}, \tau_q) = \sum_{m=1}^{M} \sum_{n=1}^{N} \left[\left(\frac{\phi_{n,m} - \phi_{n,m\,c}(a_{q,m}, \tau_q)}{\sigma(\phi_{n,m})} \right)^2 + \left(\frac{A_{n,m} - A_{n,m\,c}(a_{q,m}, \tau_q)}{\sigma(A_{n,m})} \right)^2 \right] \quad (22)$$

where a_q and τ_q are the fractions and lifetimes of the different fluorescence components, respectively, $\phi_{n,m}$ and $A_{n,m}$ are phase shift and modulation calculated from the experimental data in the mth pixel and nth frequency, and $\sigma(\phi_{n,m})$ and $\sigma(A_{n,m})$ are their estimated standard deviations. Expressions $\phi_{n,m\,c}(a_{q,m}, \tau_q)$ and $A_{n,m\,c}(a_{q,m}, \tau_q)$ stand for calculated phase shift and modulation values given by a proposed model [49].

Verveer et al. [49] showed that global analysis achieves better accuracy than pixel-by-pixel analysis methods because it uses signals from many pixels to determine the decay characteristics. Especially for low signal-to-noise ratios, which can be the case in many biological FLIM measurements, global analysis might be preferable. Verveer et al. applied global analysis to frequency-domain FLIM data but they assumed that global analysis could be applied also for time-domain measurements [49].

Based on linear fitting and global analysis, Clayton et al. developed a graphical method to estimate the lifetimes of two components from single-frequency FLIM data [50]. In their method, the measured phase and demodulation values were transformed to represent linear functions of the two components' populations. Lifetime values were determined

from points where the linear fit of the data crosses with a half circle going through points (0, 0), (1, 0) and (½ , ½). Clayton et al. mentioned that such models of two components with single-exponential decay estimations are often good enough for biological samples. [50] It should be kept in mind though that some real-life examples are more heterogenous and require therefore multiexponential decay estimates.

4.1.4 Bayesian analysis

Bayesian methods apply probabilities to determine likely values for unknown parameters based on given evidence. In Bayesian analysis of FLIM data, a prior distribution of the fluorescence decay and a likelihood function are designed to find out a posterior distribution. Estimated parameters are iterated until the posterior distribution is maximised. [5] The aim is to describe how likely a photon is detected at a particular time point [51].

Let us assume that there is a data set, D, and a set of model parameters, θ, that describe a fluorescence decay model. The prior distribution can be defined as the probability $p(\theta)$, and the likelihood function as the probability $p(D|\theta)$. The marking $p(D|\theta)$ indicates the probability of *D* given that θ has taken place. [52] The posterior distribution $p(\theta|D)$ tells the probability of the model parameters given that the measured data has occurred, and it relates to the likelihood function and the prior distribution as follows [52]:

$$p(\theta|D) \propto p(D|\theta) \times p(\theta) \tag{23}$$

Hence, the goal in Bayesian analysis is to find out probabilities of different model parameter sets and so define the most likely set of parameters from experimental data [52].

Moreover, Bayesian analysis can be used to select between different physical models. In the case of fluorescence, for instance, two models can be used. The first model H_{sig} describes the fluorescence signal and the second model H_{bg} describes the background noise. Bayesian analysis then aims to find out the probability of a signal being present in a data set D as follows [53]:

$$p\left(H_{sig}\middle|D\right) = \frac{p(D|H_{sig})p(H_{sig})}{p(H_{sig})p(D|H_{sig})+p(H_{bg})p(D|H_{bg})} \tag{24}$$

The equation tells the probability of how likely the data set D contains information of the fluorescence that fits to the signal model H_{sig}. [53]

Several FLIM analysis approaches based on Bayesian analysis have been developed, and these methods seem to work well also for FLIM data with low count rates and signal-to-noise ratios. For instance, Barber et al. [53] described a Bayesian analysis method for detecting fluorescence bursts from signals that include background noise. Their method

was able to identify fluorescence bursts in situations where 90 % of the signal amplitude came from background and only 10 % from fluorescence. From the distinguished burst data, fluorescence lifetimes could be estimated [53]. In another example study, Rowley et al. [51] showed that Bayesian analysis gives more accurate lifetime estimates for very low count rates than least square analysis, maximum likelihood estimation or phasor analysis. Their analysis functioned with high background levels as well. Kaye et al. [52] developed further the model of Rowley et al. presented in [51] to take into account biexponential decays. Kaye et al. tested their method with FRET experiments and demonstrated that it performs well with both low photon counts and low fraction regimes [52].

4.2 Phasor method

As a fit-free analysis example, phasor method is introduced next. The phasor method does not apply any designed exponential models to the data but instead, uses the phase ϕ and modulation M of the fluorescence signal directly for analysis [54]. The fluorescence decay parameters of each pixel are converted into a vector-like phasor of a two-dimensional space [5]. The phase ϕ determines the angle of the pointer in the phasor space while the degree of modulation M determines the length of the pointer [4]. The pointers of each pixel are collected in a phasor plot which is a display of $M\sin(\phi)$ versus $M\cos(\phi)$ [16,54]. A phasor plot example is shown in Figure 15.

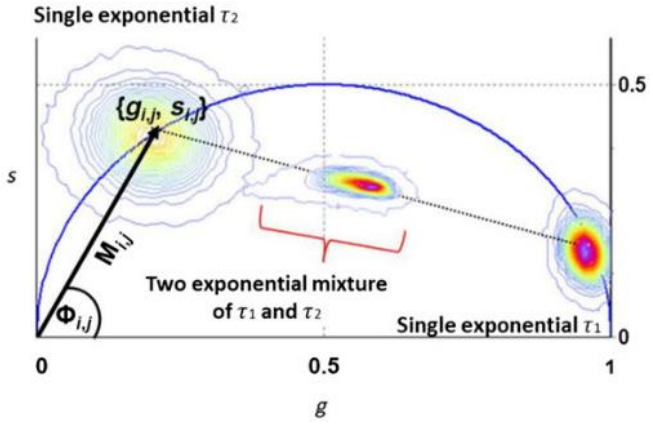

Figure 15. *Phasor plot example. One individual phasor is shown as a black arrow. Phasor clusters of two single exponential lifetimes τ_1 and τ_2 are plotted on the blue semicircle. Inside the semicircle, there is an example of a two-exponential mixture of τ_1 and τ_2.* [5]

As can be seen from Figure 15, the phasor location in the plot depends on the fluorescence lifetime [4]. For a single exponential decay, the relationship between phasor coordinates g and s, and the fluorescence lifetime are given by [54]

$$g_{i,j}(\omega) = \frac{1}{1+(\omega\tau)^2} \tag{25}$$

and

$$s_{i,j}(\omega) = \frac{\omega\tau}{1+(\omega\tau)^2} \tag{26}$$

where indexes i and j identify pixel coordinates, ω is the excitation angular frequency, and τ the fluorescence lifetime. In the case of multiexponential decay, phasor coordinates are the following [54]:

$$g_{i,j}(\omega) = \sum_k \frac{f_k}{1+(\omega\tau_k)^2} \tag{27}$$

and

$$s_{i,j}(\omega) = \sum_k \frac{f_k\omega\tau_k}{1+(\omega\tau_k)^2} \tag{28}$$

where f_k is the intensity weighted fraction of the kth component with lifetime τ_k.

It is recognized that the fluorescence decay type can be estimated from the phasor plot. Signals originating from single exponential decays are plotted on a semicircle with a center at (1/2, 0) and a radius of ½ [54]. Points from multiexponential decay land inside the semicircle, as seen in Figure 15. If the decay includes several processes, as for example in FRET, the point is plotted outside of the semicircle [4]. Short lifetimes have small phase angles and correspond therefore to phasors close to the point (1, 0). Longer lifetimes have larger phase angles, hence correspond to phasors closer to the point (0, 0). [54] Thus, pixels with similar lifetime values group together in the phasor plot [5].

According to Digman et al. [54], every molecule has its own characteristic phasor. Therefore, molecules in a sample can be identified by their position in the phasor plot. Digman et al. showed that calculations of absolute lifetimes are unnecessary when identifying molecular species in a sample, determining molecular fractions in a pixel, or calculating FRET efficiencies. If necessary, however, lifetime values can be determined as well. [54]

An advantage of the phasor approach is that it is a fit-free analysis method and therefore useful also for large lifetime data sets. Its visual representation is simple to understand and good for presenting also heterogenous lifetimes. [5] Even though the phasor method is often applied for frequency-domain data, it can be applied for time-domain data as well [54]. The phasor coordinates are got from Fourier transformation of the time-domain decay curves in each pixel. For instance, Fereidouni et al. presented a modified phasor analysis suitable for time gated FLIM data [30]. Moreover, their analysis method was capable to discriminate two lifetime components from their measurements even though time gated data is often insufficient for determining multiexponential decays. Downsides of the phasor method are its poor accuracy for low signal-to-noise data, and its sensitivity for instrument response errors [5].

5. CHEMICAL SENSING APPLICATIONS

The discussion of different FLIM approaches in this thesis has indicated the suitability of fluorescence lifetime imaging for biological applications. Fluorophores are not anymore used only to label molecules or stain cells but are also applied to visualize the chemical composition of their environment [55]. As already mentioned previously, fluorophore characteristics depend on their molecular environment. Interactions between a fluorophore and an analyte molecule lead often to changes in a fluorophore's quantum efficiency and fluorescence lifetime [10]. FLIM can be used to detect these changes and that way to quantify analyte concentrations. Thus, FLIM can be applied to get information about dynamic changes in microenvironments.

Environmental changes can have significant impact on cell behaviour and survival which is why environmental conditions of cell studies need to be controlled carefully. FLIM has offered accurate methods to visualize cellular conditions and monitor environmental changes with high temporal and spatial resolution. Therefore, FLIM is more and more applied in cell biology and has become a powerful tool for chemical sensing. Current FLIM applications range from autofluorescence and acidity measurements to temperature and viscosity sensing, just to mention some [5]. Next, lifetime-based oxygen measurements are discussed, after which other FLIM-based sensing applications such as ion concentration, pH, and FRET measurements are reviewed shortly.

5.1 Oxygen level measurements

Oxygen level measurements with FLIM take advantage of a phenomenon called photoluminescence quenching where energy is transferred from an excited fluorophore to an analyte molecule. Oxygen (O^2) has a tendency to quench phosphorescence emission. In the quenching process O^2 collides with an indicator fluorophore molecule that has ended up in its lowest excited triplet state. The collision results in an energy transmission from indicator to O^2: the indicator returns from its excited triplet state to ground state while O^2 goes from ground state to its excited state [56]. The decay of the indicator is radiationless because of the energy transfer to O^2. Therefore, when no O^2 is present, the fluorophores are excited after which they go back to the ground state without any quenching interactions and emit phosphorescence where no energy is lost. However, when O^2 is present, it can interact with triplet state fluorophores so that a part of the energy otherwise emitted via phosphorescence is transferred from dye to O^2, leading to

loss of phosphorescence. In other words, when O^2 concentration increases, phosphorescence intensity and lifetime decrease.

Because now phosphorescence is discussed, it is more accurate to talk about phosphorescence lifetime imaging microscopy (PLIM) than about FLIM. Anyhow, the principles reviewed in this thesis count as much for PLIM as for FLIM. PLIM is a convenient method to detect changes in phosphorescence lifetime that result from quenching by oxygen. Measured phosphorescence lifetimes can be converted into O^2 concentrations by using a Stern-Volmer equation. The Stern-Volmer equation describes the relation between phosphorescence lifetime and the present O^2 concentration [57]:

$$\frac{\tau_0}{\tau} = 1 + Ksv[O_2] = 1 + kq\tau_0[O_2] \tag{29}$$

In the equation, τ_0 denotes the emission decay lifetime in the absence of oxygen and τ denotes the emission decay lifetime at the present oxygen concentration, $[o_2]$ is the present oxygen concentration, k_q is the quenching rate constant, and K_{SV} is the Stern–Volmer quenching constant. [57] So, after phosphorescence lifetimes are measured with PLIM, the corresponding O^2 concentrations can be calculated as follows:

$$[O_2] = (\tau_0 - \tau)/(\tau * Ksv) \tag{30}$$

An experimental calibration curve can be constructed by measuring phosphorescence lifetimes at different known O^2 levels. The data is then fitted to a function to describe the relationship between O^2 concentration and phosphorescence intensity or lifetime [56]. One example of an oxygen calibration curve is presented in Figure 16.

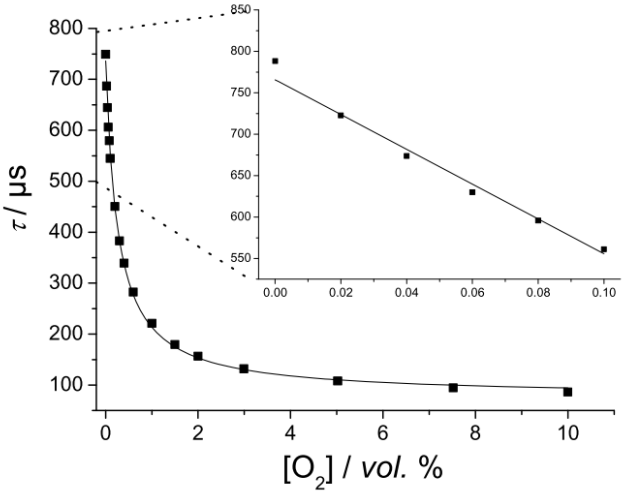

Figure 16. *Calibration curve for oxygen concentration determination from phosphorescence lifetime measurements.* [58]

In this calibration curve example, phosphorescence lifetimes were measured with phase modulation spectroscopy and plotted as a function of O^2 concentration. By fitting a function curve to the measurement points, the O^2 concentration can be determined at any lifetime measured. [58]

As current research is shifting from 2D cell cultures to 3D cell and tissue models, the need of proper 3D imaging approaches is rising also from the oxygen sensing point of view. Recently phosphorescent micro- and nanoparticles have been introduced as an option for 3D oxygen monitoring. Several types of microparticles have been tested in studies ranging from measuring intracellular oxygen concentrations [59,60] and monitoring oxygen levels in 3D cell cultures [58,60–62], to applying them in organ-on-a-chip devices [63–65]. These studies have in common, that they determined oxygen concentrations via phosphorescence lifetime measurements. For instance, Dmitriev et al. [60] used phosphorescent nanoparticles to measure oxygen concentrations in primary neural cell cultures, neural 3D cell aggregates and brain tissue slices. Phosphorescence lifetime data was collected with a confocal microscopy setup with a TCSPC hardware. Phosphorescence lifetimes were calculated with a single-exponential decay fit, and converted into corresponding oxygen concentrations with an appropriate calibration function. [60]

5.2 Other applications

In addition to oxygen concentration measurements, FLIM can be applied for sensing of several other chemical compounds as well. One commonly used approach is to measure ion concentrations. There are, for instance, fluorescent indicators for calcium (Ca^{2+}), magnesium (Mg^{2+}), zinc (Zn^{2+}) sodium (Na^{+}) and potassium (K^{+}) ions [55]. Chloride (Cl^{-}) concentrations have also been mapped with FLIM by determining lifetimes of Cl^{-} -sensitive fluorophores. As in the case of oxygen, Cl^{-} sensing is based on quenching processes that follow the Stern-Volmer kinetics [2].

Ca^{2+} is one of the most studied ions in cell biology because it takes part in many significant signalling pathways and cellular processes. Therefore, it is no wonder that several fluorescent probes for Ca^{2+} have been developed. In FLIM, Ca^{2+} experiments have been performed for example with Oregon Green Bapta-1 (OGB1), Oregon Green Bapta-2 (OGB2), and Oregon Green Bapta-5N (OGB5N) dyes [22]. Agronskaia et al. [22] examined these dyes with a widefield FLIM setup based on time-gating and used OGB1 in Ca^{2+} imaging experiments of beating neonatal rat myocytes. They found out that OGB1 and OGB2 function well in Ca^{2+} concentrations between 1 nM to 500 nM whereas OGB5N could be used up to 3 µM Ca^{2+} concentrations. [22] More recently, Zheng et al.

[66] applied OGB1 in FLIM to monitor intracellular Ca^{2+} concentrations in individual cells of an acute brain slice with a two-photon microscope including TCSPC instrumentation. An example image of their data is shown in Figure 17. Besides OGB-dyes there are also other Ca^{2+}-sensitive indicators compatible with fluorescence lifetime measurements. For instance, Jahn & Hille [67] characterized Asante Calcium Red (ACR) and Asante Calcium Green (ACG) with a TCSPC-based two-photon microscope setup and used the ACR to record dopamine-induced Ca^{2+}-fluctuations in salivary duct cells.

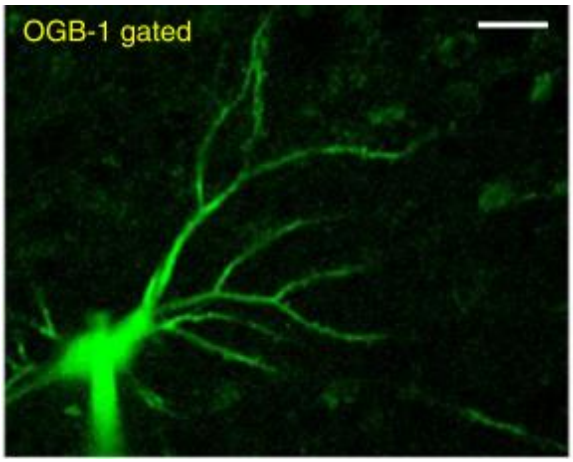

Figure 17. *An image of a pyramidal cell stained with the calcium-sensitive fluorescence dye Oregon Green Bapta-1 (OGB1), acquired with a TCSPC-FLIM setup.* [66]

It seems that less FLIM experiments have been done with Na^+-sensitive fluorophores than with Ca^{2+}-sensitive dyes even though Na^+ has also important cellular tasks. Still, there are some examples of fluorophores which fluorescence lifetimes change depending on the surrounding Na^+ concentration. Sodium Green is one such Na^+-sensitive probe. Sodium Green characterization done by Szmacinski & Lakowicz [68] showed a clear Na^+-dependency in the dye's fluorescence decay and demonstrated that Sodium Green could be used to record intracellular Na^+ concentrations with FLIM.

Recently, another Na^+-sensitive fluorescent sensor dye, CoroNaGreen, was characterized by Meyer et al. [69]. TCSPC-based FLIM measurements done with human embryonic kidney cells revealed that the fluorescence lifetime of CoroNaGreen increased when the intracellular Na^+ increased, indicating that CoroNaGreen could be a valuable tool for further Na^+-FLIM experiments [69]. Figure 18 gives insight to the CoroNaGreen lifetime experiments, showing how the fluorescence lifetime changes when the Na^+ concentration is increased.

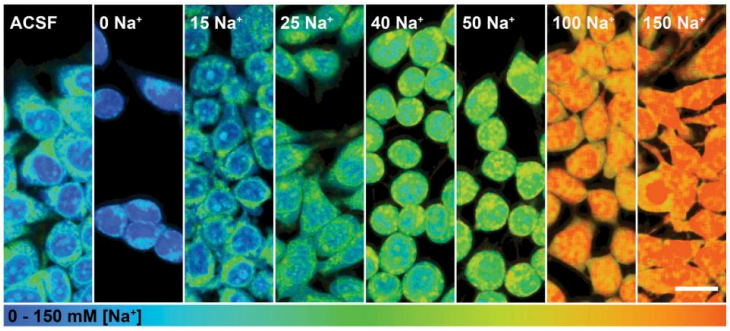

Figure 18. *FLIM images of CoroNaGreen-loaded human embryonic kidney cells at different sodium concentrations. The higher the ion concentration, the longer (in the image more red) the fluorescence lifetime.* [69]

In addition to metal ion sensing, FLIM has been utilized in pH measurements. The idea of applying FLIM to determine pH levels is based on fluorophores that have different lifetimes in their protonated and deprotonated forms. The equilibrium between these two forms depends on the current pH. Therefore, the detected fluorescence lifetime is also pH-dependent. [10] Examples of such pH-sensitive fluorophores are Carboxy- (C-) SNAFL1, C-SNAFL2, fluorescein, and C-fluorescein, all having their own fluorescence lifetime sensitive pH range [70].

Several studies have proved FLIM's suitability for spatial and temporal pH measurements. For example, Lin et al. [70] applied FLIM to measure intracellular pH values. Their setup was based on a homodyne frequency-domain FLIM and included a gain-modulated image intensifier coupled with a CCD camera. Three different cell types were labelled with C-SNAFL2 and imaged for determining pH values in cytosol and lysosomes. A clamping method was used to determine pH calibration curves. Weak bases, weak acids, ionophores and proton pump inhibitors were used to cause pH changes in the cells. The pH fluctuations were successfully observed in the FLIM measurements, showing that the technique could monitor pH levels inside cells. [70]

An additional widely spread application of FLIM in biological research is detection of FRET. FRET is a phenomenon where an excited donor molecule transfers energy non-radiatively to a ground state acceptor molecule. This interaction causes quenching of the donor's fluorescence. [2] It can take place only if the spectral emission of the donor overlaps with the spectral absorption of the acceptor and if the donor and acceptor molecules are very close to each other, typically at a distance smaller than 10 nm. [3, p. 14] Thus, FRET can be applied to test molecular distances on very small scales. For instance, if one protein is labelled with a donor fluorophore and another protein with an acceptor fluorophore, the detection of FRET reveals close proximity and possible interactions of these proteins [2]. This principle of FRET is presented in Figure 19.

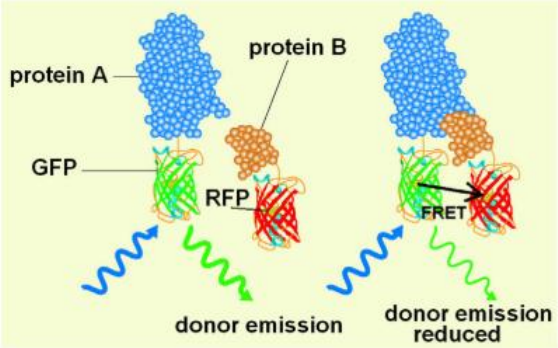

Figure 19. *An illustration of the principle of Förster Resonance Energy Transfer (FRET). Protein A is labelled with a green fluorescent protein (GFP) and protein B with a red fluorescent protein (RFP). If proteins A and B are close enough, FRET takes place between GFP and RFP which leads to quenching of GFP's emission.* [2]

The number of FLIM-FRET studies has risen constantly during the recent years. In addition to detect protein interactions, FLIM-FRET measurements have been done to observe conformational changes in proteins, to detect changes in cellular second messenger levels, and to monitor developmental events in cells [71]. To give some more examples, Andrews et al. applied FRET to visualize apoptotic events in transgenic zebrafish larvae [47], and Zhao et al. used FRET to monitor Ca^{2+} and cyclic adenosine monophosphate levels in live zebrafish embryos [72].

6. CONCLUSIONS

Fluorescence lifetime is a feature of a fluorescent molecule that describes how long the molecule spends in its excited state. In other words, it is the time constant of a molecule's fluorescence decay function [4]. Fluorescence Lifetime Imaging Microscopy takes advantage of this lifetime property to obtain biological information at the molecular scale. FLIM is non-invasive, independent of fluorophore intensity variations, and sensitive to changes in a fluorophore's molecular environment [8]. Thus, it can provide accurate data about interactions between a fluorophore and its environment.

In this thesis, FLIM techniques and implementation options have been examined. We saw that fluorescence lifetime can be examined in both time- and frequency-domain. Time and frequency domains are related to each other via a Fourier transform, and thus measure the same phenomenon but only from two perspectives. Therefore, both domains should end up in same lifetime values. Most used time-domain based FLIM methods are TCSPC and time gating. For frequency-domain measurements, homodyne and heterodyne methods can be applied. This thesis reviewed the principles of these time- and frequency-domain FLIM techniques and reflected their advantages and disadvantages. A comparison of the different approaches is summarized in Table 2.

Commonly, widefield FLIM applications have utilized time-gating or frequency-domain methods based on gated or modulated image intensifiers whereas scanning FLIM applications have applied TCSPC or frequency-domain measurements with gain-modulated photomultiplier tubes. However, development that has taken place during recent decades shows that much more setup combinations can be used. One interesting development is to implement TCSPC with widefield illumination so that the lifetime accuracy and single photon sensitivity of TCSPC are combined with advantages of widefield imaging.

In addition to time- and frequency-domain principles, this thesis gave insight on current FLIM implementations by reviewing widefield-FLIM, confocal-FLIM and multiphoton-FLIM examples. Even though widefield imaging reaches faster acquisition times than scanning microscopes, it lacks inherent optical sectioning capability. Additional instrumentation can enable 3D imaging with conventional widefield microscopes but more commonly, confocal and multiphoton microscopes are utilized because they include optical sectioning possibilities themselves.

Table 2. *Comparison of different FLIM techniques*

FLIM TECHNIQUE	ADVANTAGES	DISADVANTAGES	REFERENCES
TCSPC	- time resolution up to picoseconds - single photon sensitivity → good performance with low intensity samples - high lifetime accuracy - good signal-to-noise ratio - wide dynamic range - good performance with multiexponential decays as well	- slow acquisition - electronic dead times around 100-350 ns, - requires complex instrumentation (e.g. pulsed lasers), - data amounts huge → memory constrains - not optimal with high photon count rates → results in pile up	[2,4,5,8,9,26]
TIME GATE	- faster data acquisition than in TCSPC - electronic dead times short: under 1 ns - high count rates around 10 MHz range	- less accurate - lower time resolution - undersampling can be an issue due to limited number of gates - lower photon efficiency because of gating - not optimal for multiexponential decays	[2,5,7,8,71]
FREQUENCY DOMAIN	- fast data acquisition - good photon efficiency - no pulsed lasers required - no detector saturation - good performance with high intensity samples due to analog measurements	- lower signal-to-noise ratio compared to time-domain methods - analysis more complex - can suffer from aliasing - not optimal for low photon counts	[5,8,14,71]

While 3D cell culturing and tissue engineering get more popular in the research world, there is an increasing need for new and better 3D imaging techniques. Although 3D FLIM can be achieved with confocal and multiphoton microscopes, they start to be slow and less sensitive when sample sizes and imaging depths increase. Therefore, FLIM implementation to SPIM and OPT has been examined recently to achieve better imaging of cell behaviour in context to their 3D environment. In this thesis, several FLIM implementations to SPIM and OPT were discussed. Based on the studies, it seems that CCD cameras are a suitable choice for SPIM-FLIM and OPT-FLIM. On the other hand, CMOS camera development has brought up alternatives for CCD-based detectors. It might be that CMOS cameras could provide a wider range of implementation possibilities, including widefield TCSPC. Therefore, CMOS cameras are also strong candidates for SPIM-FLIM and OPT-FLIM setups.

The selection of a suitable data acquisition technique and detection system depends on what the performance goals of the FLIM experiment are. For instance, desired signal-to-noise ratio, photon rate from the sample, number of decay components, photon efficiency of the detection system, desired time resolution and lifetime accuracy are parameters that affect the choice of which techniques should be used. In addition, an appropriate analysis method needs to be selected. It is often the case that, independent of the methods used, noise and background signals are present in FLIM data which can make it difficult to recognize small lifetime changes. Effective analysis methods can help to obtain desired results and even improve performance of the used system.

This thesis has provided insight to different FLIM methods, implementations, and analysis tools. It has shown that FLIM is a widely used tool and has already many applications in chemical sensing and cellular biology. Here, FLIM-based oxygen sensing, ion concentration measurements, pH monitoring, and FRET experiments were introduced. FLIM has already turned out to be an important tool for biomedical research. Anyhow, it seems that there is still uncovered potential in FLIM and plenty of new application possibilities to be studied, especially in the area of 3D experiments. Future development might reveal even faster and more accurate FLIM methods for life science.

REFERENCES

[1] Lichtman JW, Conchello JA, Fluorescence microscopy, Nature Methods, 2005, Vol. 2, No. 12, pp. 910–919.

[2] Suhling K, Hirvonen LM, Levitt JA, Chung PH, Tregidgo C, Le Marois A, Rusakov DA, Zheng K, Ameer-Beg S, Poland S, Coelho S, Henderson R, Krstajic N, Fluorescence lifetime imaging (FLIM): Basic concepts and some recent developments, Medical Photonics, 2015, Vol. 27, pp. 3–40.

[3] Periasamy A, Clegg RM, FLIM Microscopy in Biology and Medicine, CRC Press/Taylor & Francis Group, Boca Raton, USA, 2009, 407 p.

[4] Becker W, Fluorescence lifetime imaging - techniques and applications, Journal of Microscopy, 2012, Vol. 247, No. 2, pp. 119–136.

[5] Datta R, Heaster TM, Sharick JT, Gillette AA, Skala MC, Fluorescence lifetime imaging microscopy: fundamentals and advances in instrumentation, analysis, and applications, Journal of Biomedical Optics, 2020, Vol. 25, No. 7, pp. 1–43.

[6] Rivera KR, Yokus MA, Erb PD, Pozdin VA, Daniele M, Measuring and regulating oxygen levels in microphysiological systems: Design, material, and sensor considerations, Analyst, 2019, Vol. 144, p. 3190–3215.

[7] Lakowicz JR, Principles of Fluorescence Spectroscopy, Third Edition, Springer Science+Business Media, New York, USA, 2006, 954 p.

[8] Liu X, Lin D, Becker W, Niu J, Yu B, Liu L, Qu J, Fast fluorescence lifetime imaging techniques: A review on challenge and development, Journal of Innovative Optical Health Science, 2019, Vol. 12, No. 5, pp. 1–27.

[9] Becker W, Bergmann A, Hink MA, König K, Benndorf K, Biskup C, Fluorescence Lifetime Imaging by Time-Correlated Single-Photon Counting, Microscopy Research and Technique, 2004, Vol. 63, No. 1, pp. 58–66.

[10] Becker W, Fluorescence lifetime imaging by multi-dimensional time correlated single photon counting, Medical Photonics, 2015, Vol. 27, pp. 41–61.

[11] Phillips D, Christensen RL, Time Correlated Single-Photon Counting (Tcspc) Using Laser Excitation, Instrumentation Science & Technology, 1985, Vol. 14, No. 3–4, pp. 267–292.

[12] Image Intensifiers, Hamamatsu Photonics K.K., Literature Number: TII 0007E02,

May 2020, 19 p. Available: https://www.hamamatsu.com/resources/pdf/etd/II_TII0007E.pdf.

[13] Gratton E, Breusegem S, Sutin J, Ruan Q, Barry N, Fluorescence lifetime imaging for the two-photon microscope: time-domain and frequency-domain methods, Journal of Biomedical Optics, 2003, Vol. 8, No. 3, pp. 381–390.

[14] Gadella TWJ, Van Hoek A, Visser AJWG, Construction and characterization of a frequency-domain fluorescence lifetime imaging microscopy system, Journal of Fluorescence, 1997, Vol. 7, No. 1, pp. 35–43.

[15] Chandler DE, Majumdar ZK, Heiss GJ, Clegg RM, Ruby crystal for demonstrating time- and frequency-domain methods of fluorescence lifetime measurements, Journal of Fluorescence, 2006, Vol. 16, pp. 793–807.

[16] Buranachai C, Kamiyama D, Chiba A, Williams BD, Clegg RM, Rapid frequency-domain flim spinning disk confocal microscope: Lifetime resolution, image improvement and wavelet analysis, Journal of Fluorescence, 2008, Vol. 18, pp. 929–942.

[17] Spring BQ, Clegg RM, Image analysis for denoising full-field frequency-domain fluorescence lifetime images, Journal of Microscopy, 2009, Vol. 235, No. 2, pp. 221–237.

[18] Chen H, Holst G, Gratton E, Using of a modulated CMOS camera for fluorescence lifetime microscopy, Microscopy Research and Technique, 2015, Vol. 78, No. 12, pp. 1075-1081.

[19] Ulku AC, Bruschini C, Antolovic IM, Kuo Y, Ankri R, Weiss S, Michalet X, Charbon E, A 512 × 512 SPAD image sensor with integrated gating for widefield FLIM, IEEE Journal of Selected Topics in Quantum Electronics, 2019, Vol. 25, No. 1, pp. 1–38.

[20] Ankri R, Basu A, Ulku AC, Bruschini C, Charbon E, Weiss S, Micalet X, Single-Photon, Time-Gated, Phasor-Based Fluorescence Lifetime Imaging through Highly Scattering Medium, ACS Photonics, 2020, Vol. 7, pp. 68–79.

[21] Sawosz P, Wojtkiewicz S, Kacprzak M, Zieminska E, Morawiec M, Maniewski R, Liebert A, Towards in-vivo assessment of fluorescence lifetime: imaging using time-gated intensified CCD camera, Biocybernetics and Biomedical Engineering, 2018, Vol. 38, pp. 966–974.

[22] Agronskaia A V., Tertoolen L, Gerritsen HC. Fast fluorescence lifetime imaging of calcium in living cells, Journal of Biomedical Optics, 2004, Vol. 9, No. 6, pp. 1230–

1237.

[23] Wu HM, Lee TA, Ko PL, Liao WH, Hsieh TH, Tung YC, Widefield frequency domain fluorescence lifetime imaging microscopy (FD-FLIM) for accurate measurement of oxygen gradients within microfluidic devices, Analyst, 2019, Vol. 144, pp. 3494–3504.

[24] Schneckenburger H, Weber P, Wagner M, Bruns T, Richter V, Schickinger S, Wittig R, Multidimensional fluorescence microscopy in live cell imaging - A mini review, Photonics and Lasers in Medicine, 2012, Vol. 1, pp. 35–40.

[25] Cole MJ, Siegel J, Webb SED, Jones R, Dowling K, Dayel MJ, Parsons-Karavassilis D, French PMW, Lever MJ, Sucharov LOD, Neil MAA, Juskaitis R, Wilson T, Time-domain whole-field fluorescence lifetime imaging with optical sectioning, Journal of Microscopy, 2001, Vol. 203, No. 3, pp. 246–257.

[26] Suhling K, Hirvonen LM, Becker W, Smietana S, Netz H, Milnes J, Conneely T, Le Marois A, Jagutzki O, Festy F, Petrásek Z, Beeby A, Wide-field time-correlated single photon counting-based fluorescence lifetime imaging microscopy, Nuclear Instruments and Methods in Physics Research, Section A, 2019, Vol. 942, pp. 162365–162372.

[27] Schoutteten L, Denjean P, Pansu RB, Characterisation of a Time resolved Photon Counting Confocal Fluorescence Microscope, Journal of Fluorescence, 1997, Vol. 7, No. 2, pp. 155–165.

[28] Booth MJ, Wilson T, Low-cost, frequency-domain, fluorescence lifetime confocal microscopy, Journal of Microscopy, 2004, Vol. 214, No. 1, pp. 36–42.

[29] Gerritsen HC, Asselbergs MA, Agronskaia AV, Van Sark WG, Fluorescence lifetime imaging in scanning microscopes: acquisition speed, photon economy and lifetime resolution, Journal of Microscopy, 2002, Vol. 206, No. 3, pp. 218–224.

[30] Fereidouni F, Esposito A, Blab GA, Gerritsen HC, A modified phasor approach for analyzing time-gated fluorescence lifetime images, Journal of Microscopy, 2011, Vol. 244, No. 3, pp. 248–258.

[31] Coelho S, Poland SP, Devauges V, Ameer-Beg SM, Adaptive optics for a time-resolved Förster resonance energy transfer (FRET) and fluorescence lifetime imaging microscopy (FLIM) in vivo, Optics Letters, 2020, Vol. 45, No. 10, pp. 2732–2735.

[32] Becker W, Su B, Holub O, Weisshart K, FLIM and FCS detection in laser-scanning microscopes: Increased efficiency by GaAsP hybrid detectors, Microscopy

Research and Technique, 2011, Vol. 74, pp. 804–811.

[33] Zhang Y, Khan AA, Vigil GD, Howard SS, Super-sensitivity multiphoton frequency-domain fluorescence lifetime imaging microscopy, Optics Express, 2016, Vol. 24, No. 18, pp. 20862–20867.

[34] Bruschini C, Homulle H, Antolovic IM, Burri S, Charbon E, Single-photon avalanche diode imagers in biophotonics: review and outlook, Light: Science & Applications, 2019, Vol. 8, pp. 87–115.

[35] Mitchell AC, Wall JE, Murray JG, Morgan CG, Direct modulation of the effective sensitivity of a CCD detector: a new approach to time-resolved fluorescence imaging, Journal of Microscopy, 2002, Vol. 206, No. 3, pp. 225–232.

[36] Li DD-U, Arlt J, Tyndall D, Walker R, Richardson J, Stoppa D, Charbon E, Henderson RK, Video-rate fluorescence lifetime imaging camera with CMOS single-photon avalanche diode arrays and high-speed imaging algorithm, Journal of Biomedical Optics, 2011, Vol. 16, No. 9, pp. 096012-1–096012-12.

[37] Burri S, Powolny F, Bruschini C, Michalet X, Regazzoni F, Charbon E, A 65k pixel, 150k frames-per-second camera with global gating and micro-lenses suitable for fluorescence lifetime imaging, Proceedings of SPIE International Society for Optical Engineering, 2014, Vol. 9141, pp. 914109–914122.

[38] Greger K, Neetz MJ, Reynaud EG, Stelzer EHK, Three-dimensional Fluorescence Lifetime Imaging with a Single Plane Illumination Microscope provides an improved Signal to Noise Ratio, Optics Express, 2011, Vol. 19, No. 21, pp. 20743–20750.

[39] Abu-Siniyeh A, Al-Zyoud W, Highlights on selected microscopy techniques to study zebrafish developmental biology, Laboratory Animal Research, 2020, Vol. 36, No. 1, pp. 12–22.

[40] Funane T, Hou SS, Zoltowska KM, Van Veluw SJ, Berezovska O, Kumar ATN, Bacskai BJ, Selective plane illumination microscopy (SPIM) with time-domain fluorescence lifetime imaging microscopy (FLIM) for volumetric measurement of cleared mouse brain samples, Review of Scientific Instruments, 2018, Vol. 89, No. 5, pp. 053705-1–053705-8.

[41] Hirvonen LM, Nedbal J, Almutairi N, Phillips TA, Becker W, Conneely T, Milnes J, Cox S, Stürzenbaum S, Suhling K, Lightsheet fluorescence lifetime imaging microscopy with wide-field time-correlated single photon counting, Journal of Biophotonics, 2019, Vol. 13, pp. 1–10.

[42] Li R, Liu A, Wu T, Xiao W, Tang L, Chen L, Digital scanned laser light-sheet fluorescence lifetime microscopy with wide-field time-gated imaging, Journal of Microscopy, 2020, Vol. 279, No. 1, pp. 69–76.

[43] Mitchell CA, Poland SP, Seyforth J, Nedbal J, Gelot T, Huq T, Holst G, Knight RD, Ameer-Beg SM, Functional in vivo imaging using fluorescence lifetime light-sheet microscopy, Optics Letter, 2017, Vol. 42, No. 7, pp. 1269–1272.

[44] Sharpe J, Optical projection tomography, In: Sensen CW and Hallgrímsson (eds.), Advanced Imaging in Biology and Medicine: Technology, Software Environments, Applications, Springer-Verlag, Berlin Heidelberg, Germany, 2009, pp. 199–224.

[45] Godavarty A, Sevick-Muraca EM, Eppstein MJ, Three-dimensional fluorescence lifetime tomography, Medical Physics, 2005, Vol. 32, No. 4, pp. 992–1000.

[46] McGinty J, Tahir KB, Laine R, Talbot CB, Dunsby C, Neil MAA, Quintana L, Swoger J, Sharpe J, French PMW, Fluorescence lifetime optical projection tomography, Journal of Biophotonics, 2008, Vol. 1, No. 5, pp. 390–394.

[47] Andrews N, Ramel MC, Kumar S, Alexandrov Y, Kelly DJ, Warren SC, Kerry L, Lockwood N, Frolov A, Frankel P, Bugeon L, McGinty J, Dallman MJ, French PMW, Visualising apoptosis in live zebrafish using fluorescence lifetime imaging with optical projection tomography to map FRET biosensor activity in space and time, Journal of Biophotonics, 2016, Vol. 9, No. 4, pp. 414–424.

[48] Maus M, Cotlet M, Hofkens J, Gensch T, De Schryver FC, Schaffer J, Seidel CAM, An experimental comparison of the maximum likelihood estimation and nonlinear least-squares fluorescence lifetime analysis of single molecules, Analytical Chemistry, 2001, Vol. 73, No. 9, 2078–2086.

[49] Verveer PJ, Squire A, Bastiaens PIH, Global analysis of fluorescence lifetime imaging microscopy data, Biophysical Journal, 2000, Vol. 78, No. 4, pp. 2127–2137.

[50] Clayton AHA, Hanley QS, Verveer PJ, Graphical representation and multicomponent analysis of single-frequency fluorescence lifetime imaging microscopy data, Journal of Microscopy, 2004, Vol. 213, No. 1, pp. 1–5.

[51] Rowley MI, Barber PR, Coolen ACC, Vojnovic B, Bayesian analysis of fluorescence lifetime imaging data, Multiphoton Microscopy in the Biomedical Sciences XI, Proceedings of SPIE, 2011, Vol. 7903, pp. 790325-1–790325-12.

[52] Kaye B, Foster PJ, Yoo TY, Needleman DJ, Developing and testing a bayesian analysis of fluorescence lifetime measurements, PLoS One, 2017, Vol. 12, No. 1,

pp. 1–13.

[53] Barber PR, Ameer-Beg SM, Pathmananthan S, Rowley M, Coolen ACC, A Bayesian method for single molecule, fluorescence burst analysis, Biomedical Optics Express, 2010, Vol. 1, No. 4, pp. 1148–1158.

[54] Digman MA, Caiolfa VR, Zamai M, Gratton E, The phasor approach to fluorescence lifetime imaging analysis, Biophysical Journal: Biophysical Letters, 2008, Vol. 94, No. 2, pp. 14–16.

[55] Schäferling M, The art of fluorescence imaging with chemical sensors, Angewandte Chemie - International Edition, 2012, Vol. 51, pp. 3532–3554.

[56] Ast C, Schmälzlin E, Löhmannsröben HG, van Dongen JT, Optical oxygen micro- and nanosensors for plant applications, Sensors (Switzerland), 2012, Vol. 12, pp. 7015–7032.

[57] Feng Y, Cheng J, Zhou L, Zhou X, Xiang H, Ratiometric optical oxygen sensing: A review in respect of material design, Analyst, 2012, Vol. 137 p. 4885–4901.

[58] Steinbrück D, Schmälzlin E, Peinemann F, Kumke MU, An innovative laser-based sensing platform for realtime optical monitoring of oxygen, In: 14th Joint International IMEKO TC1, TC7, TC13 Symposium, Jena, Germany, August 31–September 2, 2011, pp. 207–211.

[59] Schmälzlin E, Van Dongen JT, Klimant I, Marmodée B, Steup M, Fisahn J, Geigenberger P, Löhmannsröben H-G, An optical multifrequency phase-modulation method using microbeads for measuring intracellular oxygen concentrations in plants, Biophysical Journal, 2005, Vol. 89, No. 2, pp. 1339–1345.

[60] Dmitriev RI, Borisov SM, Kondrashina A V., Pakan JMP, Anilkumar U, Prehn JHM, Zhdanov AV, McDermott KW, Klimant I, Papkovsky DB, Imaging oxygen in neural cell and tissue models by means of anionic cell-permeable phosphorescent nanoparticles, Cellular and Molecular Life Sciences, 2015, Vol. 72, pp. 367–381.

[61] Lesher-Pérez SC, Kim GA, Kuo CH, Leung BM, Mong S, Kojima T, Moraes C, Thouless MD, Luker GD, Takayama S, Dispersible oxygen microsensors map oxygen gradients in three-dimensional cell cultures, Biomaterials Science, 2017, Vol. 5, pp. 2106–2113.

[62] Weyand B, Nöhre M, Schmälzlin E, Stolz M, Israelowitz M, Gille C, von Schroeder HB, Reimers K, Vogt PM, Noninvasive oxygen monitoring in three-dimensional tissue cultures under static and dynamic culture conditions, Bioresearch Open

Access, 2015, Vol. 4, No. 1, pp. 266–277.

[63] Ehrlich A, Tsytkin-Kirschenzweig S, Ioannidis K, Ayyash M, Riu A, Note R, Ouedraogo G, Vanfleteren J, Cohen M, Nahmias Y, Microphysiological flux balance platform unravels the dynamics of drug induced steatosis, Lab on a Chip, 2018, Vol. 18, No. 17, pp. 2510–2522.

[64] Sonntag F, Schmieder F, Ströbel J, Grünzner S, Busek M, Günther K, Steege T, Polk C, Klotzbach U, Universal lab-on-a-chip platform for complex, perfused 3D cell cultures, In: Microfluidics, BioMEMS, and Medical Microsystems XIV, Proceedings of SPIE, 2016, Vol. 9705, pp. 970516-1–970516-12.

[65] Busek M, Grünzner S, Steege T, Klotzbach U, Sonntag F, Hypoxia-on-a-chip, Current Directions in Biomedical Engineering, 2016, Vol. 2, No. 1, pp. 71–75.

[66] Zheng K, Jensen TP, Rusakov DA, Monitoring intracellular nanomolar calcium using fluorescence lifetime imaging, Nature Protocols, 2018, Vol. 13, No. 3, pp. 581–597.

[67] Jahn K, Hille C, Asante calcium green and asante calcium red - Novel calcium indicators for two-photon fluorescence lifetime imaging, PLoS One, 2014, Vol. 9, No. 8, pp. 105334-1–105334-13.

[68] Szmacinski H, Lakowicz JR, Sodium green as a potential probe for intracellular sodium imaging based on fluorescence lifetime, Analytical Biochemistry, 1997, Vol. 250, pp. 131–138.

[69] Meyer J, Untiet V, Fahlke C, Gensch T, Rose CR, Quantitative determination of cellular [Na+] by fluorescence lifetime imaging with CoroNaGreen, Journal of General Physiology, 2019, Vol. 151, No. 11, pp. 1319–1331.

[70] Lin HJ, Herman P, Lakowicz JR, Fluorescence Lifetime-Resolved pH Imaging of Living Cells, Cytometry Part A, 2003, Vol. 52, No. 2, pp. 77–89.

[71] De Los Santos C, Chang C-W, Mycek M-A, Cardullo RA, FRAP, FLIM, and FRET: Detection and Analysis of Cellular Dynamics on a Molecular Scale Using Fluorescence Microscopy, Molecular Reproduction and Development, 2015, Vol. 82, pp. 587–604.

[72] Zhao M, Wan X, Li Y, Zhou W, Peng L, Multiplexed 3D FRET imaging in deep tissue of live embryos, Scientific Reports, 2015, Vol. 5, pp. 13991-1–13991-15.